ELSEVIER

Journal of Structural Geology 28 (2006) 1422–1444

JOURNAL OF STRUCTURAL GEOLOGY

www.elsevier.com/locate/jsg

Relationships between melt-induced rheological transitions and finite strain: Observations from host rock pendants of the Tuolumne Intrusive Suite, Sierra Nevada, California

Markus Albertz*

Department of Earth Sciences, University of Southern California, Los Angeles, CA 90089-0740, USA

Received 15 December 2005; received in revised form 1 April 2006; accepted 4 April 2006
Available online 21 June 2006

Abstract

Finite strain analysis in the northern (Piute Meadow pendant (PMP)) and eastern (Saddlebag Lake pendant (SLP)) host rock pendants of the Tuolumne Intrusive Suite (TIS) reveals plane strain geometries in the pendants and a steep strain gradient in the SLP. Average regional *z*-axis shortening in both pendants is ca. 43% and increases to ca. 70 and 85% in the SLP within ca. 100 m to the pluton contact. Microstructures in the SLP adjust to increasing temperatures and partial melting near the margin. Beyond the pluton margin, weakly elongate quartz grains with lobate grain boundaries, patchy to sweeping undulose extinction, deformation bands, and incipient subgrains are consistent with low-temperature dislocation creep. Towards the margin, quartz grain boundaries become increasingly irregular and display ''chessboard'' patterns indicating high-temperature dislocation creep. Grain size is markedly smaller near the margin and despite large finite strain grains do not show evidence for crystal-plastic deformation. Cuspate strain-free interstices are interpreted to mimic former anatectic melt. Outcrop-scale migmatization, coincidence with abruptly increasing finite strain, and microfracturing towards the margin implies that fracture-induced mechanical grain size reduction may have triggered the transition to melt-assisted granular flow, ultimately resulting in drastic rheological weakening.

Keywords: Finite strain; Rheological weakening; Melt-assisted granular flow; Tuolumne Intrusive Suite; Saddlebag Lake; Transpression

1. Introduction

Rheological modification of the lithosphere by the presence of partial melt has been inferred from numerous field and experimental studies (e.g., Davidson et al., 1992; Hollister, 1993; Tommasi et al., 1994; Neves et al., 1996; Kohlstedt, 1992; Rutter, 1997; Rosenberg and Handy, 2000, 2005). Whereas partial melting may in some cases result in hardening of surrounding rocks, for example by partitioning of water into the melt phase (e.g., Karato, 1986), melt-related rheological weakening is likely to have major large-scale tectonic consequences (Hollister and Crawford, 1986; Beaumont et al., 2001, 2004; Aoya et al., 2005). This paper is concerned with melt-induced rheological weakening.

Insight into mechanical aspects of rheological weakening in partially melted rocks has been gained as the result of laboratory experiments (e.g., Rushmer, 1995; Rutter and Neumann, 1995; Rosenberg and Handy, 2005). It is now generally accepted that once a critical amount of melt has formed in a partially melted rock, its strength reduces drastically (e.g., Rutter, 1997), and that this can lead to the initiation of shear zones (e.g., Rosenberg, 2001). However, most deformation experiments of partially melted rocks were performed for only a few percent shortening but syn-magmatic deformation of the crust may involve several tens or even hundreds percent shortening. Hence, it is fair to

* Present address: Department of Oceanography, Dalhousie University, 1355 Oxford Street, Halifax, Nova Scotia, B3H 4J1, Canada. Tel.: +1 902 494 6300; fax: +1 902 494 3877.
E-mail address: markus.albertz@dal.ca

0191-8141/$ - see front matter © 2006 Elsevier Ltd. All rights reserved.
doi:10.1016/j.jsg.2006.04.001

say that relatively little is known about the quantitative relationships of finite strain and microstructures of melt-bearing rocks in nature.

One of the best natural laboratories to evaluate finite strain and microstructures of melt-bearing rocks are aureoles of syntectonic plutons, because: (1) magma emplacement establishes temperature gradients; (2) metamorphic reactions record temperature changes in compositionally suitable rock types; (3) finite strains commonly increase towards pluton margins; (4) gradients in rheologically critical parameters (temperature, stress, fluids, strain rate) are likely to induce transitions in deformation mechanisms; and (5) points (1)–(4) can be investigated along pluton margin-perpendicular transects.

This study investigates the contributions from melt-absent and melt-present deformation mechanisms to the total finite strain in host rock pendants of the Tuolumne Intrusive Suite (TIS), California. The results of quantitative finite strain analysis and microscopic observations suggest that abruptly increasing finite strain coincides with melt-assisted granular flow thus confirming the role of melt as an efficient mechanism of rheological weakening in nature.

2. Geologic setting

2.1. Tuolumne Intrusive Suite (TIS)

The ca. 2000 km^2 large (map area), horizontally elongate TIS (Fig. 1) has long been considered the type intrusive suite representing voluminous Mesozoic magmatism in the Sierra Nevada (e.g., Bateman and Chappell, 1979; Bateman, 1992). The TIS reveals normal zoning including outer mafic and inner, more felsic units. U-Pb zircon ages for several of these units indicate that construction of the TIS occurred from ca. 94 to 82 Ma (Kistler and Fleck, 1994; Fleck et al., 1996; Coleman and Glazner, 1997; Coleman et al., 2004). Relatively shallow emplacement depths of ca. 10 km or less have been inferred from weakly metamorphosed volcanic rocks (e.g., Bateman, 1992) and Al-in-hornblende geobarometry (Ague and Brimhall, 1988; Webber et al., 2001).

At present, little agreement exists over the emplacement history of the TIS. Bateman and Chappell (1979) proposed that individual magma pulses of the TIS solidified from the margins inward and that the remaining fluid magma episodically moved upward and outward thus expanding the magma chamber. Tikoff and Teyssier (1992) invoked a model of crustal-scale en echelon P-shear tensional bridges into which Late Cretaceous granitoids, including the TIS, were emplaced. Paterson and Vernon (1995) suggested a model of nested diapirs involving several separately evolved magma pulses to yield the zoning of the TIS. Žák and Paterson (2005) argued that fractional crystallization, magmatic stoping, and downward return flow of older magma units operated during construction of a large, temporally and spatially evolving magma chamber in the TIS. In contrast, Coleman et al. (2004) proposed that emplacement occurred incrementally by small sheets or dikes without large TIS magma chambers ever existing. Regional transpression and strike-slip partitioning are thought to have been important factors during emplacement (e.g., Tikoff and de Saint Blanquat, 1997; Tikoff et al., 2005).

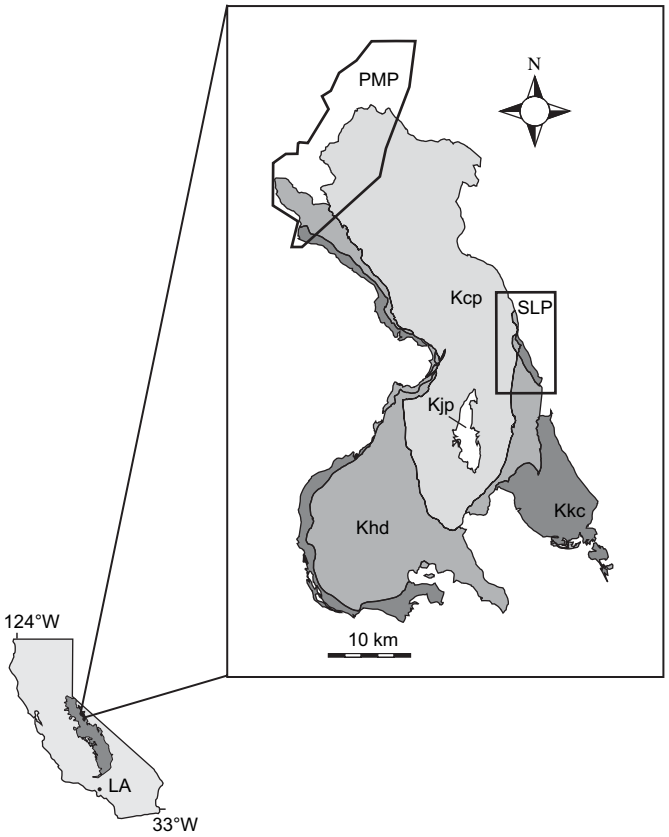

Fig. 1. Schematic geologic map of the Tuolumne Intrusive Suite (TIS), California. Kkc, Kuna Crest granodiorite; Khd, Half Dome granodiorite; Kcp, Cathedral Peak granodiorite; Kjp, Johnson Granite porphyry; PMP, Piute Meadow pendant; SLP, Saddlebag Lake pendant; LA, Los Angeles. Boxes show locations of Figs. 2 and 3.

2.2. Piute Meadow pendant (PMP)

The PMP bounds the TIS to the north (Fig. 1) and exposes a sequence of rhyolitic to dacitic and andesitic metavolcanic rocks interlayered with thin conglomerate beds in its northern part (Fig. 2A). The western part of the PMP is marked by Cretaceous granodioritic host rocks (Wahrhaftig, 2000) imbricated by reverse faults (Fig. 2B). Ample kinematic indicators, including SC-fabrics, asymmetric porphyroblasts, and offset of markers, as well as steep down-dip stretching lineations are consistent with dip-slip southwest-vergent reverse faulting. As the result of multiple episodes of regional deformation and possibly emplacement of pre-Cathedral Peak plutons, the host rocks are strongly foliated (Tobisch et al., 2000). Foliations strike NNW and dip steeply to the NNE and SSW (Fig. 2B). Local deflection of this foliation occurs in the northern aureole of the Cathedral Peak granodiorite. Stretching lineations in the host rocks consistently plunge subvertically (Fig. 2C).

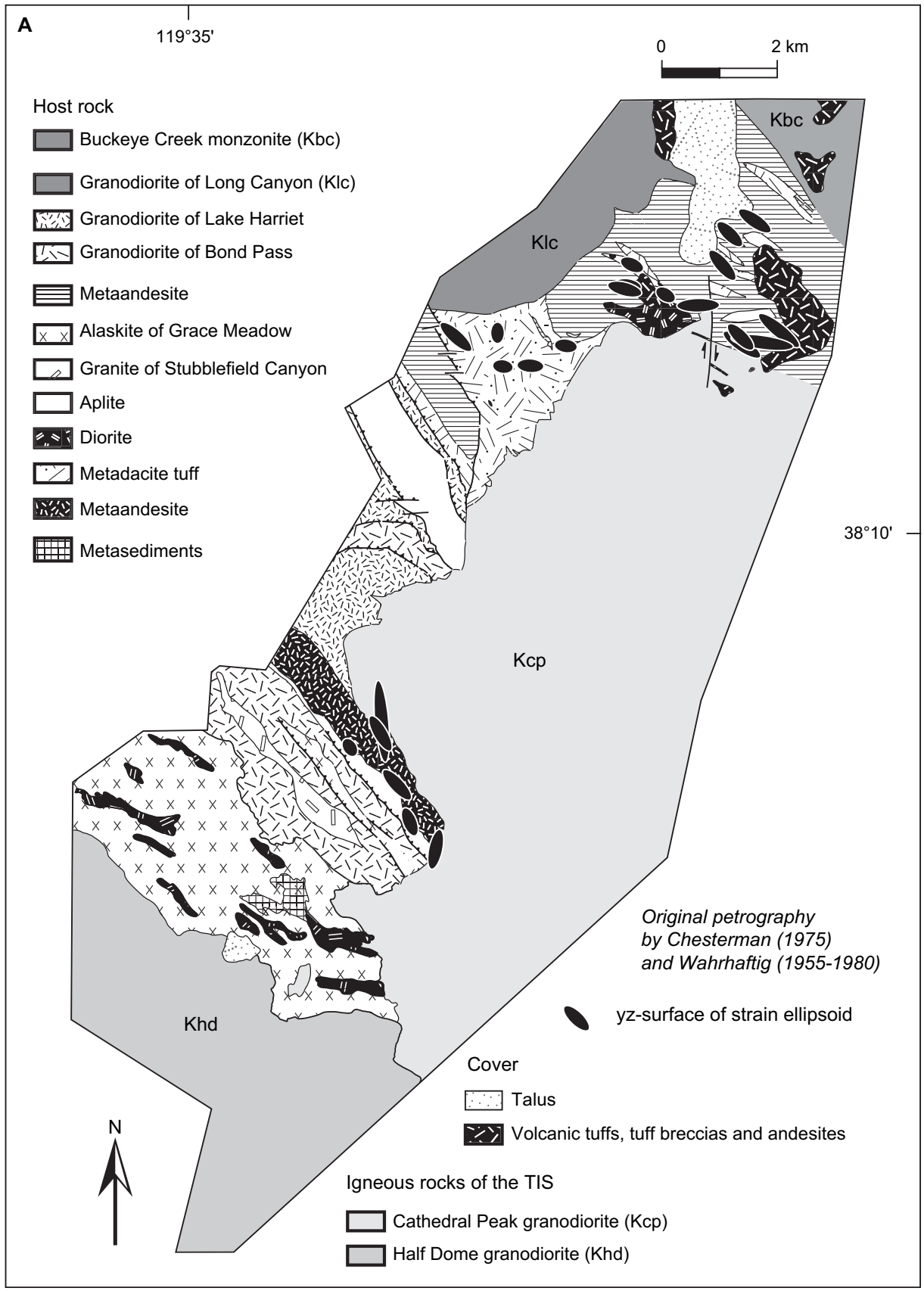

Fig. 2. (A) Geologic map of the Piute Meadow pendant (PMP). (B) Map showing planar fabrics in the PMP. (C) Map showing lineations in the PMP.

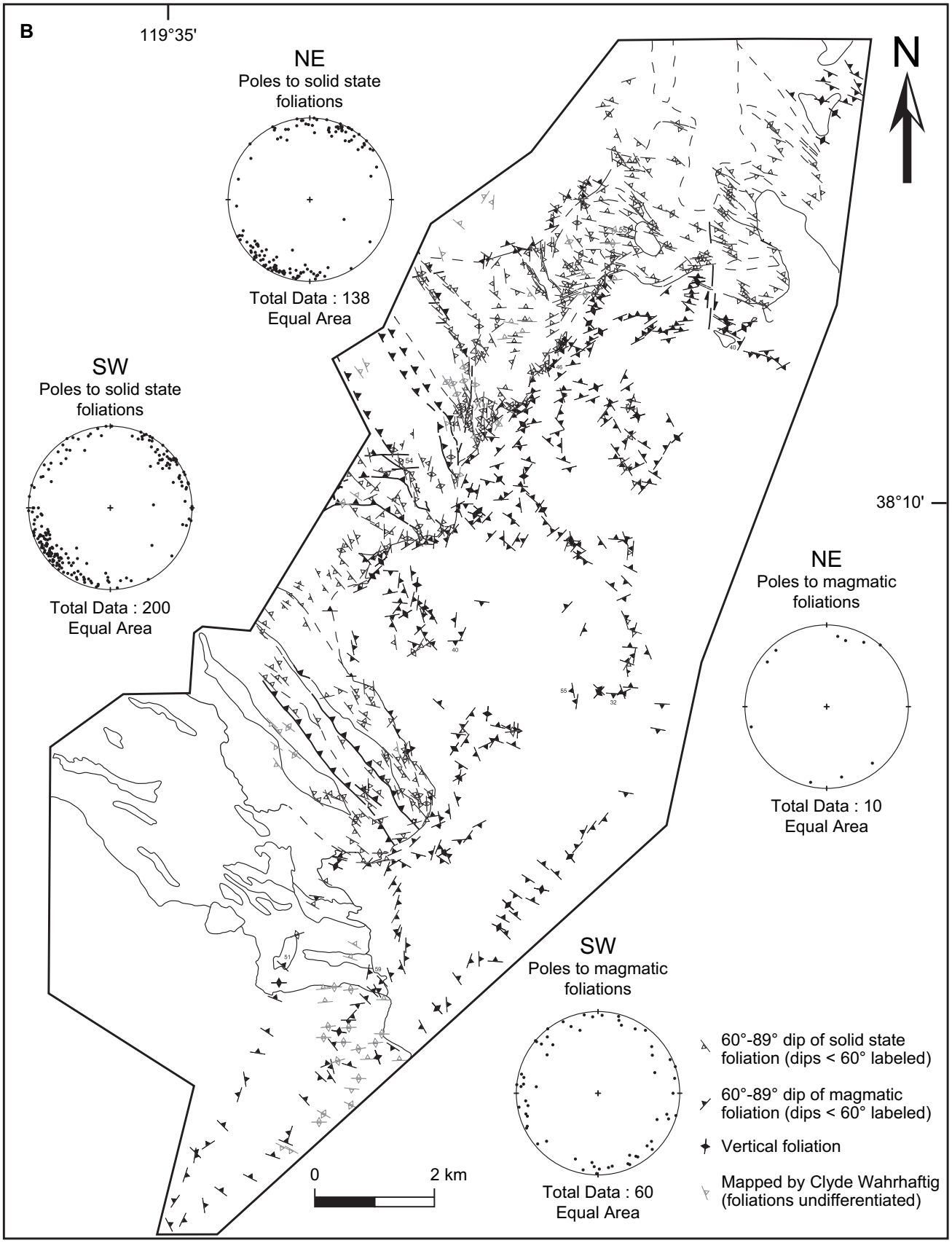

Fig. 2 (*continued*)

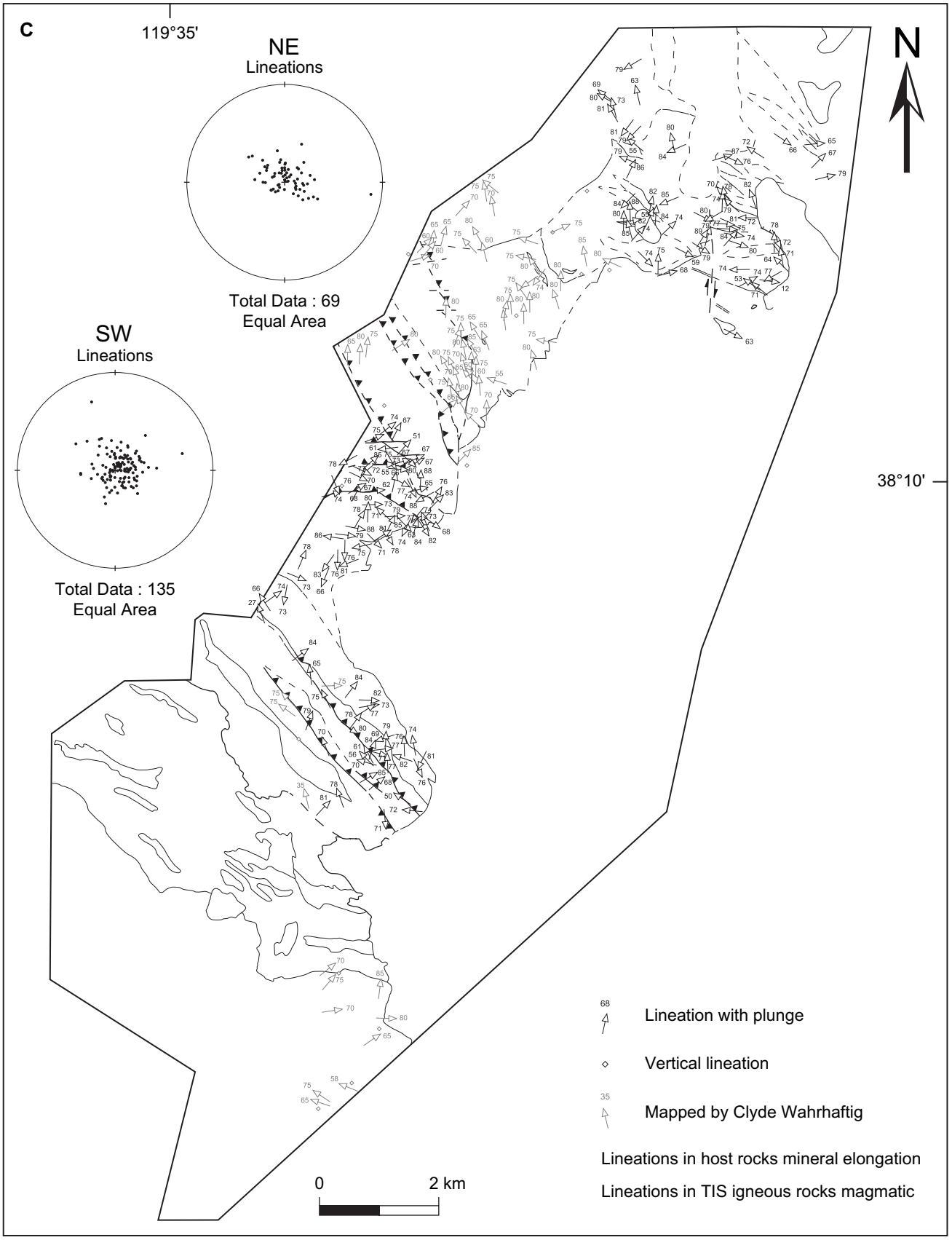

Fig. 2 (*continued*)

The pluton margin is strongly discordant to host rock markers. Pre-emplacement structures and contacts are truncated at high angle along the stepped but mostly NE-striking pluton margin. This truncation can be observed at the map and outcrop scales.

Cathedral Peak and Half Dome granodiorites are characterized by a well-developed NNW-striking magmatic foliation that parallels the regional NNW strike (Fig. 2B). Except for local maintenance of the regional orientation, the magmatic foliation swings into parallelism with the pluton margin.

2.3. Saddlebag Lake pendant (SLP)

The SLP is located at the eastern TIS margin and contains the metamorphic equivalents of rhyolites, dacites, andesites, conglomerates, sand/silt stones, and calc-silicates (Fig. 3A). Host rock bedding and contacts strike NNW thus paralleling the pluton margin. A NNW-striking and steeply NE- and SW-dipping metamorphic foliation (Fig. 3B) is most likely the result of multiple episodes of deformation (e.g., Schweickert and Lahren, 1993; Tobisch et al., 2000; Sharp et al., 2000). The host rocks are characterized by subvertical stretching lineations, locally plunging somewhat more shallowly toward the SE near the pluton contact (Fig. 3C). Though rare, kinematic indicators (asymmetric porphyroblasts, drag of lithologic contacts and structures, displacement of leucocratic dikes) indicate a pluton-side-up sense of displacement as well as domains of weakly dominantly dextral, but also sinistral, and pure shear kinematics (Albertz and Paterson, 2002).

The three major intrusive units of the TIS (Kuna Crest, Half Dome, and Cathedral Peak granodiorites) present in the SLP are characterized by a well-developed magmatic foliation. Both magmatic foliation and pluton margin are parallel to the NNW-striking regional trend of the central Sierra Nevada. The magmatic foliation crosscuts internal contacts, indicating that the foliation-forming processes postdate the juxtaposition of internal units.

The pluton margin is characterized by distinctive steps. Several isolated host rock blocks and rafts of various sizes occur within the plutonic rocks close to the contact. Block size ranges from a few cm to ca. 100 m and the long axes of blocks are typically oriented parallel to the pluton margin. Locally, migmatitic leucosomes form veins and pockets that both truncate and intrude along pre-existing host rock anisotropies. Rarely, truncated folds in metavolcanic units contain leucosomes in fold hinges (Fig. 4). Evidence for migmatization is typically found in blocks that are entirely surrounded by solidified magma, suggesting that host rock temperatures during emplacement of the TIS reached the solidus (Albertz et al., 2005).

3. Finite strain analysis

3.1. Methods

Lithic fragments, including lapilli tuffs in andesitic to rhyodacitic metavolcanics, and quartzitic to cherty components in metaconglomerates, respectively, were utilized as host rock strain markers. Prominent differences in color between felsic and more mafic compositions rendered field-based strain analysis straightforward. Dark-gray andesitic metavolcanic rocks contained abundant light-gray felsic lithic fragments, and conversely, felsic metavolcanics typically contained mafic lithic fragments. Excellent exposure conditions allowed measuring of the long and short axes of strain markers on at least two principal surfaces in the field. Whenever possible, a minimum of 30 measurements were taken per surface. In outcrops where less than 30 strain markers were present, 3–5 measurements were collected to obtain at least estimates of the finite strains. Additional data and samples were collected along two roughly ENE-striking transects in the Saddlebag Lake pendant (SLP, Fig. 3A). Quantitative strain analysis was performed in the laboratory after the samples had been prepared. Three mutually perpendicular cuts were made on each sample parallel to the principal surfaces of the fabric ellipsoids. The R_f/ϕ technique (Ramsay and Huber, 1983) and algebraic methods of Shimamoto and Ikeda (1976) were applied to calculate average two-dimensional strain ellipses for each of the three surfaces containing strain markers. Fry's (1979) center-to-center technique was used to calculate two-dimensional strain ellipses in rocks lacking strain markers. The two-dimensional strain ellipses were algebraically combined to determine the three-dimensional strain ellipsoids (Shimamoto and Ikeda, 1976). Operations were performed using software kindly provided by Scott Paterson.

The superposition of primary and tectonic fabrics may produce inaccurate finite tectonic strains (e.g., Paterson and Yu, 1994; Paterson et al., 1995). Hence, algebraic corrections were made where necessary using an average primary fabric ellipsoid derived from appropriate rock types (Wetmore and Paterson, personal communication, 2004).

The three-dimensional strain data were separated by rock type and plotted on modified Flinn diagrams using the routines of Ramsay and Huber (1983) and Twiss and Moores (1992). Logarithmic K-values were calculated to represent the shape of the strain ellipsoids by numbers (Ramsay and Huber, 1983).

3.2. Results

Figs. 2A and 3A show the yz-ellipses of the finite strain ellipsoids on map surfaces. The plotted yz-ellipses closely approximate the true orientation in the field, because the stretching lineations plunge mostly subvertically (Figs. 2C, 3C). The maps reveal that finite strain intensities are relatively constant in the PMP but increase abruptly towards the pluton margin in the SLP.

In terms of strain ellipsoid shape, the data from the Piute Meadow pendant (PMP) and Saddlebag Lake pendant (SLP) can be subdivided into three different domains (Fig. 5A): (1) a trend of moderate to high flattening strains in metavolcanics and metaconglomerates approximately parallel to the plane strain line; (2) low strains in metavolcanics plotting on the plane strain line; and (3) moderately constrictional strains calculated from several metaconglomerate samples.

The data in domain (1) suggest that differential volume loss may have occurred during plane strain deformation. For

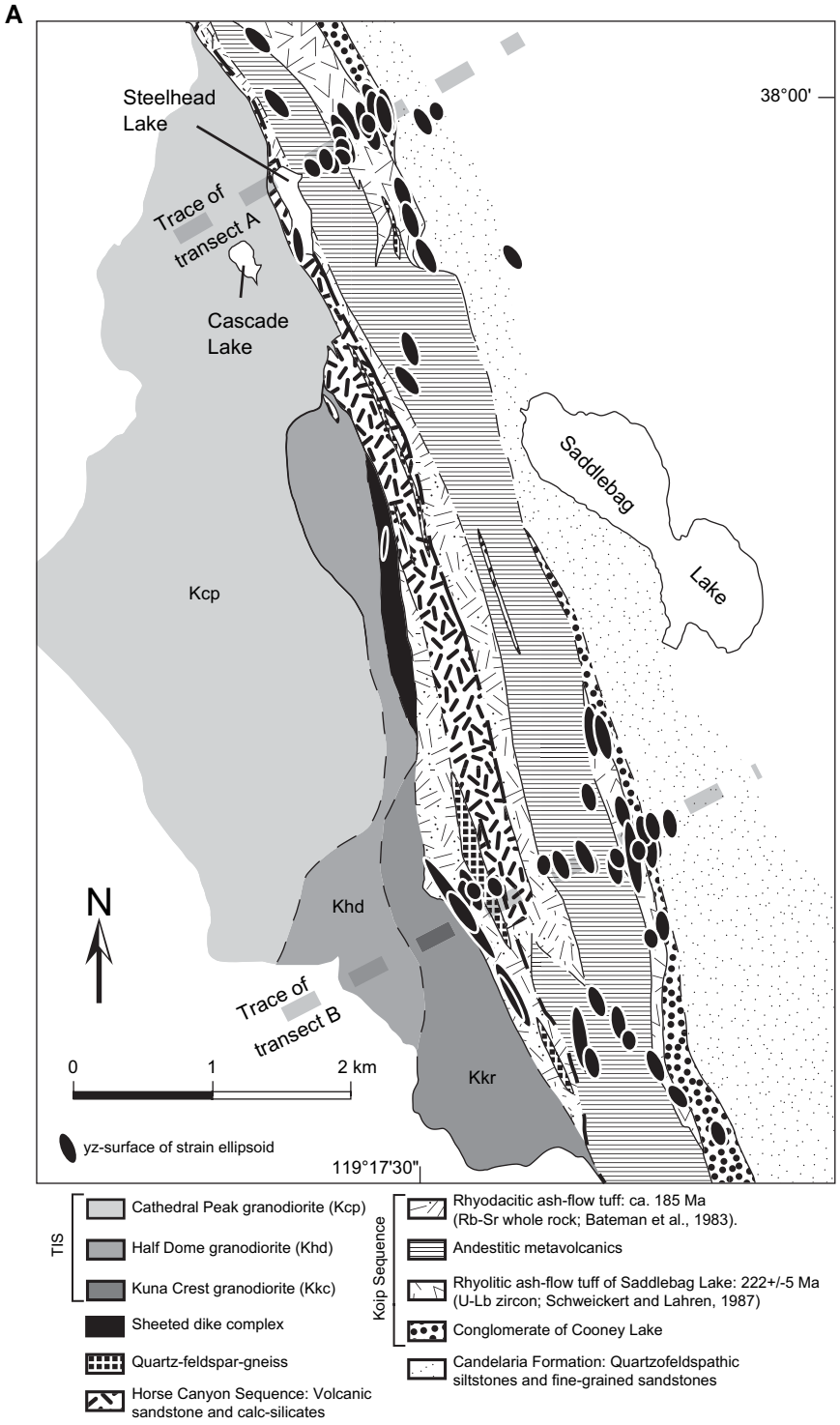

Fig. 3. (A) Geologic map of the Saddlebag Lake pendant (SLP). (B) Planar fabrics in the SLP. (C) Lineations in the SLP.

instance, Ague (1991) showed that regional metamorphism of pelites from greenschist to amphibolite facies conditions can be associated with as much as 30% volume loss. Likewise, Yoshinobu and Girty (1999) determined up to ca. 12% volume loss during contact metamorphism, indicating that in addition to volatiles, major-element mass transfer can occur during contact metamorphism. Together the two studies suggest that in some areas up to at least ca. 40% volume loss is plausible, in particular when the combined effects of regional and contact metamorphism are to be considered. The dashed lines in Fig. 5A indicate the position of the plane strain line ($k = 1$) for various amounts of differential volume loss (see routines in Ramsay and Huber (1983) and Twiss and Moores (1992)). Therefore, the strain geometries indicated for domain (1)

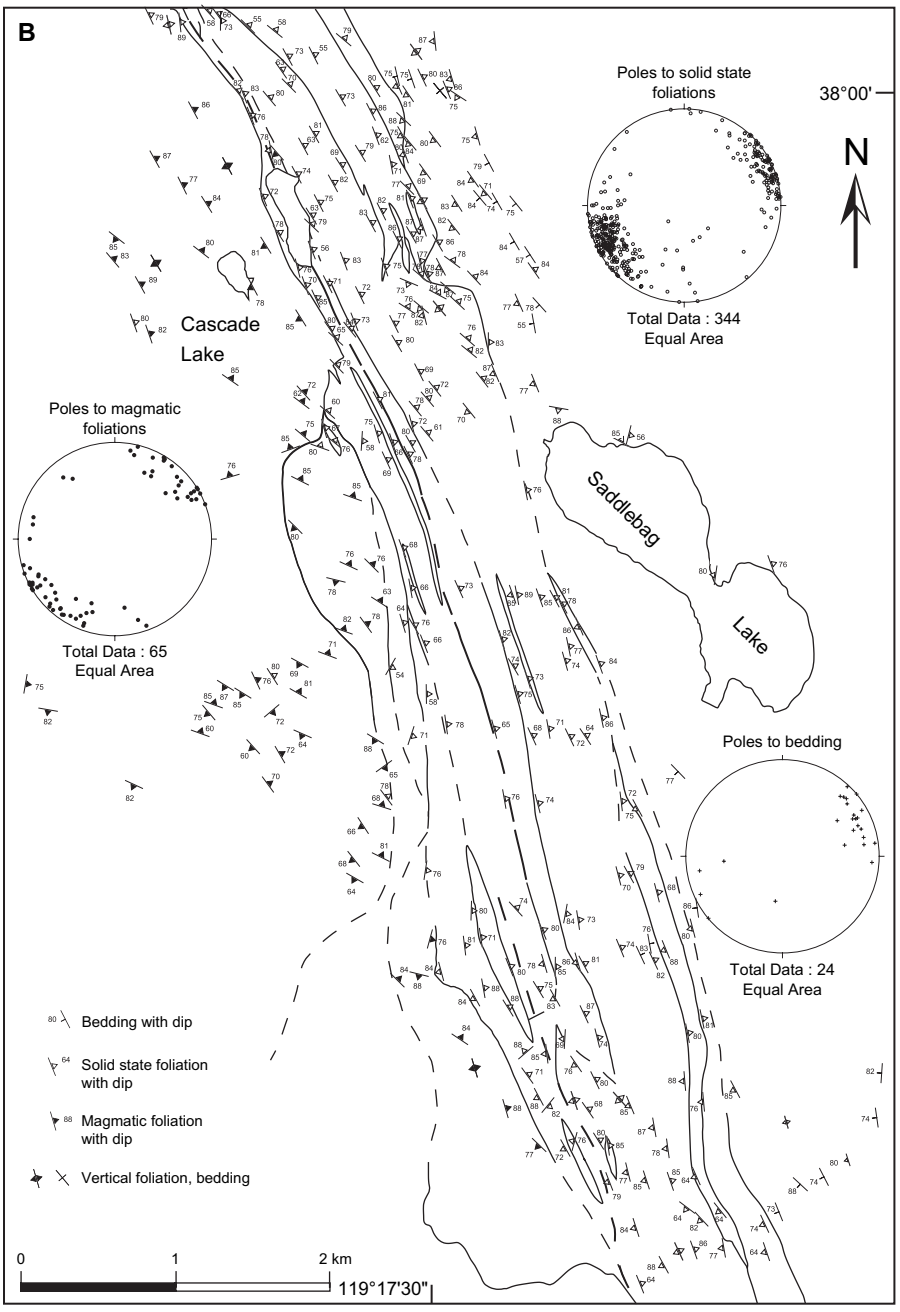

Fig. 3 (*continued*)

most likely represent apparent flattening. Shifting the plane strain line by differential volume loss yields a best fit between the data and the modified plane strain line at ca. 10–30% volume loss.

The data in domain (2) were retrieved from Fry analysis on samples lacking strain markers. Typically, these samples yielded systematically lower finite strains than those containing lithic fragments collected from adjacent outcrops. The most plausible explanation for the discrepancy in strain ellipsoid geometries between domains (1) and (2) is varying amounts of differential volume loss. As argued for domain (1), differential volume loss during overall plane strain deformation can result in apparent flattening strains. At the time of deposition, lapilli tuffs often contain gas-filled vesicles that may collapse during subsequent compaction and deformation, allowing for net volume loss. Therefore, samples that lack lithic fragments and plot in domain (2) (plane strain) may not have experienced significant amounts of differential volume loss and probably approximate the true tectonic strain.

The position of the conglomerate samples in the constrictional field (domain (3), Fig. 5A) can be explained in terms of apparent prolate fabrics associated with viscosity contrasts between the conglomerate clasts and their matrix. Freeman (1987) demonstrated through a theoretical approach that during progressive plane strain deformation of matrix-supported

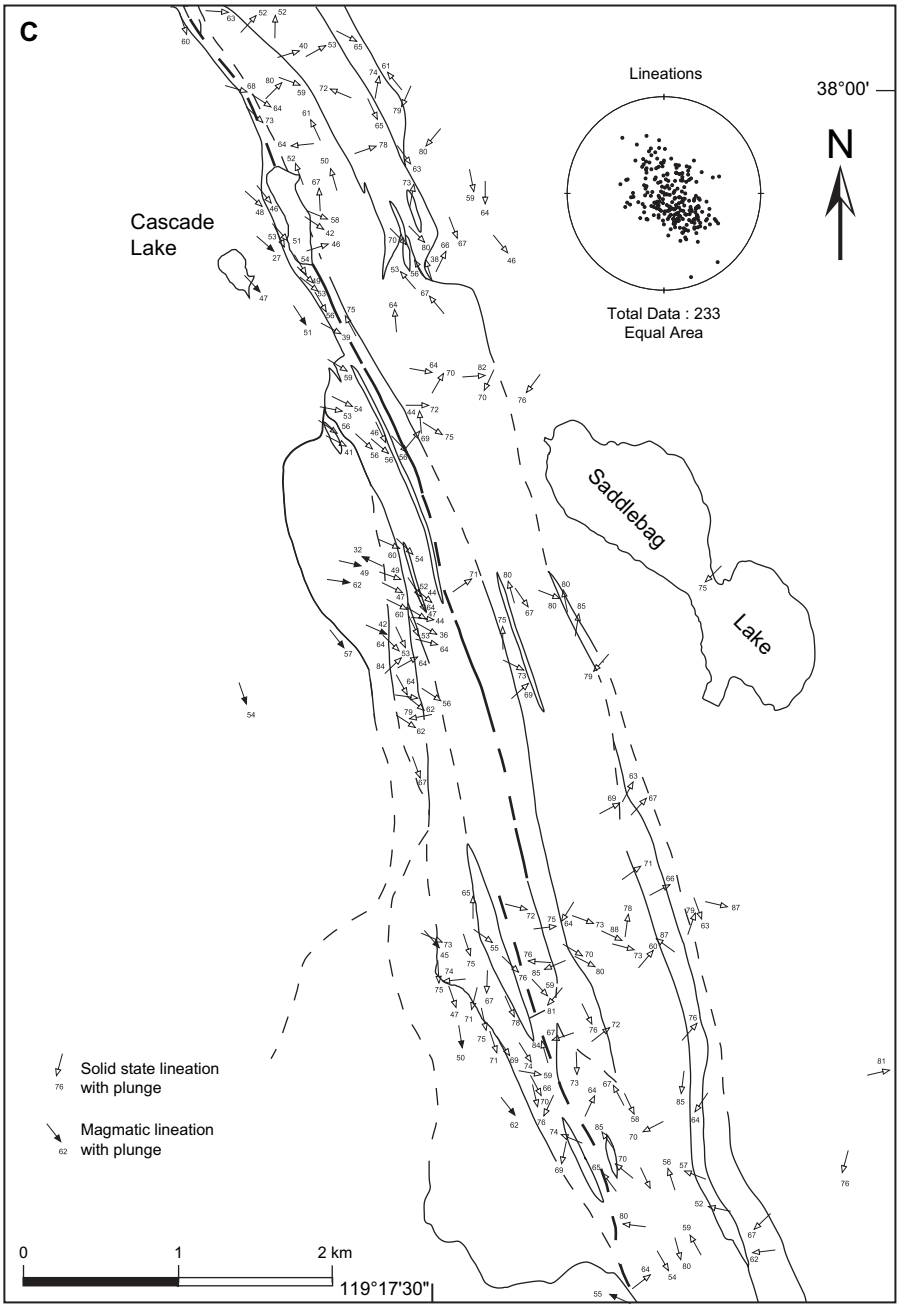

Fig. 3 (*continued*)

conglomerates, finite strains can progressively shift into the constrictional field with increasing viscosity contrasts, resulting in apparent prolate fabric ellipsoids (Fig. 5B). Field and microscopic observations on conglomerates from the SLP revealed that nearly all clasts are separated by a fine-grained groundmass, confirming that these conglomerates are matrix-supported. Additionally, some of the conglomerates with constrictional fabrics in the SLP occur in lenses interbedded with felsic and mafic metavolcanics which in turn are consistent with plane strain fabrics during volume loss (see above). Therefore, the constrictional strains of the SLP conglomerates most likely formed by progressive migration of the fabric ellipsoids into the constrictional field during overall plane strain deformation (notice how some conglomerate samples move toward more constrictional shapes perpendicular to the plane strain line (Fig. 5A)).

To quantify the strain gradient in the SLP, strain ellipsoid shapes and intensities were examined as a function of position. In spite of some scatter, the data define relatively straight lines in transects A (Fig. 6A) and B (Fig. 6B) with average K-values of ca. 0.7 to 0.9, indicating that the strain type does not change towards the pluton margin. In keeping with the corrections applied above, conglomerates with K-values larger than 1 are considered indicative of apparent constrictional strain, and apparent flattening strains derived from metavolcanics in truth probably are the result of differential volume loss during plane strain

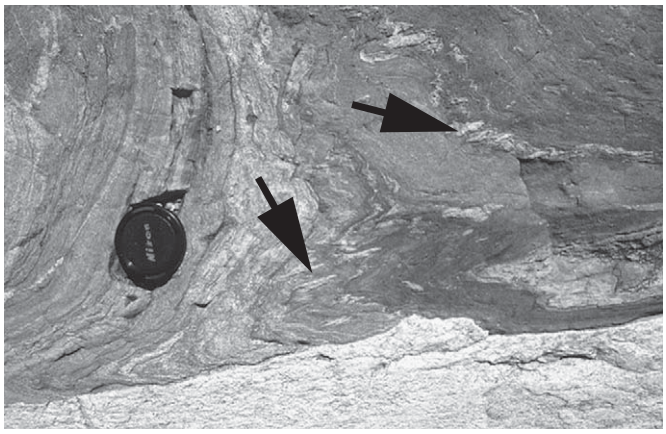

Fig. 4. Outcrop photograph of migmatites at TIS contact. Arrows indicate leucosomes intruded parallel to axial-planes of folded metavolcanic host rock. Lens cap (ca. 5 cm in diameter) for scale.

deformation. Despite constant strain ellipsoid shapes, *z*-axis shortening increases drastically towards the margin. Fig. 7 shows that background strain intensities scatter and vary from ca. 20 to ca. 65% at distances of ca. 700 and 1400 m to the pluton margin (Fig. 7A and B, respectively). Within ca. 100 m to the contact, strain intensities increase abruptly and consistently from an average background value of ca. 43% to ca. 70% (Fig. 7A) and ca. 85% (Fig. 7B), respectively. 82–83% shortening is also observed between the strain transects (Albertz et al., 2005). Closest to the pluton, low to intermediate strain intensities are absent and in general the rocks are so highly shortened that strains often cannot be quantified fully because outcrop heights are shorter than long axes of strain markers. Thus the high proximal strains are minimum estimates.

4. Microstructural observations

In order to retrieve information on deformation temperature and rheology in the Saddlebag Lake pendant (SLP), oriented host rock samples were collected along two approximately margin-normal transects (Fig. 3A). Additional samples were collected in the host rocks and pluton. Large thin sections (2 × 3 inch) were prepared from selected samples parallel to the lineation and perpendicular to the foliation. Care was taken to avoid samples marked by strong hydrothermal alteration. Metamorphic mineral assemblages generally were only rarely recognized in the metavolcanic and metasedimentary rocks and hence cannot be described systematically. Below, representative microstructures are described in detail.

4.1. Low-temperature microstructures (≥ca. 300–900 m to pluton margin)

Andalusite-bearing metasedimentary (Fig. 8A) and metavolcanic units (Fig. 8B,C) reveal grains with various degrees of weak elongation, locally bulging grain boundaries and patchy undulose extinction (Fig. 8A,B). Metavolcanic units generally exhibit well-preserved porphyritic textures (Fig. 8B,C). 3–5 mm large, subhedral to euhedral quartz and plagioclase phenocrysts are embedded in fine-grained matrices consisting of various proportions of quartz, plagioclase and subordinately biotite and muscovite as well as opaque oxides. Quartz phenocrysts typically show patchy to sweeping undulose extinction and deformation bands and/or subgrain boundaries (Fig. 8B). Plagioclase phenocrysts lack evidence for crystal-plastic creep and show en echelon microcracks resembling bookshelf structures (box in Fig. 8C). Biotite occurs as fine-grained and relatively equant grains in the matrix and in shear bands that anastomose around plagioclase (Fig. 8C). Biotite also merges into folia and locally fills fractures in plagioclase phenocrysts, indicating that neocrystallization of biotite took place during deformation.

The anastomosing pattern of biotite suggests crystal-plastic flow, consistent with temperatures above 250 °C (Passchier and Trouw, 2005). The presence of andalusite in

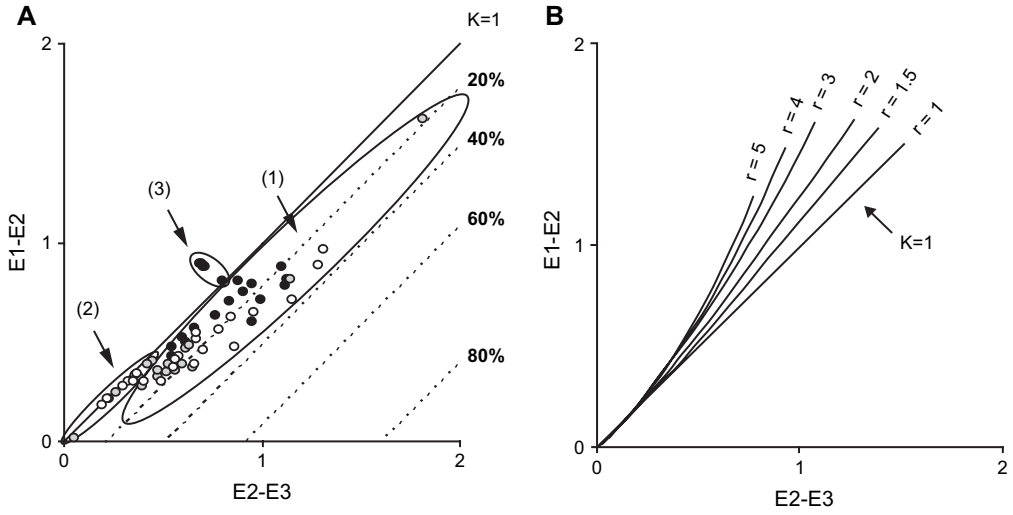

Fig. 5. (A) Modified Flinn diagram showing the strain data of this study. White dots indicate metadacites, gray dots metaandesites, and black dots conglomerates. Domains 1, 2, and 3 are outlined and labeled. Dashed lines represent position of plane strain line for various amounts of volume loss. (B) Relationship between viscosity contrast and strain ellipsoid shape (modified after Freeman, 1987).

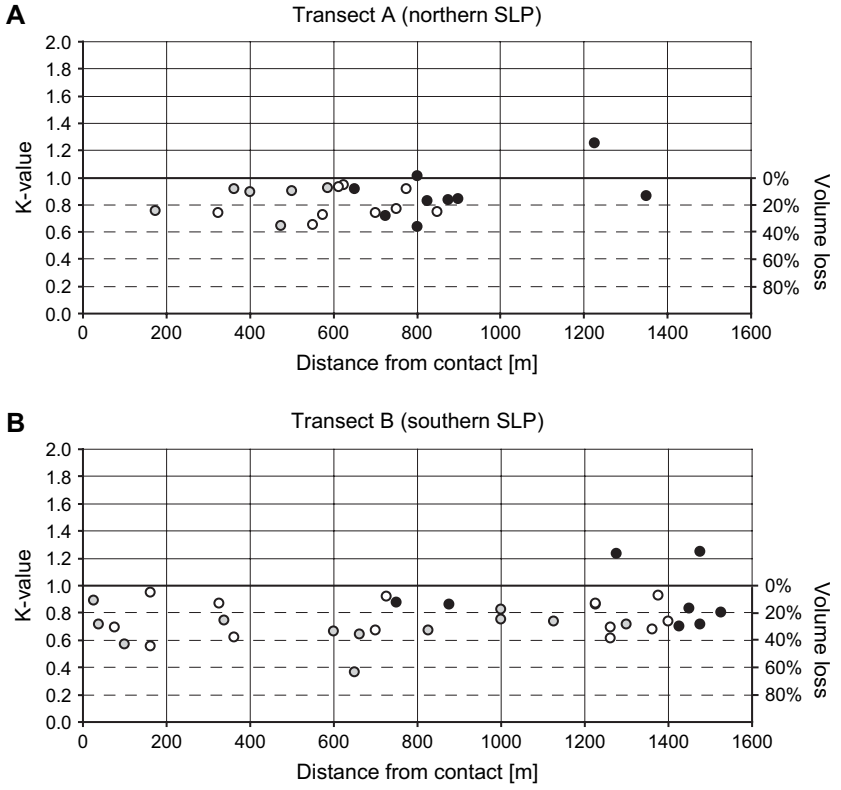

Fig. 6. Spatial distribution of *K*-values along margin-perpendicular transects A and B. White dots indicate metadacites, gray dots metaandesites, and black dots conglomerates. Bold solid line represents plane strain without volume loss. Dashed lines represent position of plane strain line for various amounts of volume loss.

metasedimentary units indicates temperatures of at least ca. 350 °C (Bohlen et al., 1991) in the pressure range of interest (2–3 kbar, Ague and Brimhall, 1988; Webber et al., 2001). The brittle imbrication of plagioclase provides an upper temperature constraint of ca. 400 °C (Passchier and Trouw, 2005).

4.2. High-temperature microstructures (between ca. 100 and 300–800 m to pluton margin)

Matrix grains of metavolcanic units are considerably larger than those in the zone of low-temperature microstructures (compare Fig. 8B and D). Matrix quartz is significantly more flattened and reveals widespread occurrence of lobate and bulging grain boundaries (Fig. 8D). Large quartz phenocrysts (3–5 mm) display highly irregular and seriate-interlobate grain margins, such as those present at the ends of the quartz phenocrysts in Fig. 8D, indicating that grain boundary migration accommodated recrystallization (Passchier and Trouw, 2005). In addition, quartz phenocrysts reveal alternating blocky ''chessboard'' extinction patterns (Fig. 8D), consistent with simultaneous operation of the prismatic (c-slip) and basal (a-slip) slip systems in quartz (Passchier and Trouw, 2005, and therein). Kruhl (1996) systematically studied quartz subgrain patterns in various metamorphic rocks and concluded that quartz ''chessboard'' patterns indicate temperatures above ca. 620–650 °C.

4.3. Melt-bearing microstructures (≤100 m to pluton margin)

Breakdown of muscovite and neocrystallization of both fibrous sillimanite and K-feldspar (Fig. 8E) suggests that the metamorphic reactions proceeded at the second sillimanite isograd (Spear, 1993). The associated temperatures during metamorphism of pelitic rocks corresponding to pressures of 2–3 kbar lie in the range of 610–630 °C (Spear, 1993).

Proximal host rock typically displays a mosaic texture. Grains are considerably smaller (0.1–0.5 mm) and mostly blocky and equidimensional (Fig. 8F, H, J, L, N, P, R). In detail, individual grain boundaries are quite irregular (Fig. 8J, N) and the grains generally lack elongation, bulging grain boundaries, subgrains, as well as evidence for pervasive grain boundary migration and significant shape-preferred orientation. Locally, 120° triple junctions and relatively straight grain boundaries between grains of the same type resemble equilibrium textures (e.g., Fig. 8P). However, microstructural observations on samples from both host rock (see below) and the pluton (Albertz et al., 2005), are incompatible with post-tectonic static recrystallization.

Using criteria to establish the former presence of melt (e.g., Rosenberg and Riller, 2000; Sawyer, 2001; Marchildon and Brown, 2002, and therein), the following observations suggest partial melting near the TIS margin. Interstices between quartz and feldspar are filled with quartz and/or feldspar locally showing weak undulose extinction (Fig. 8F) or are completely

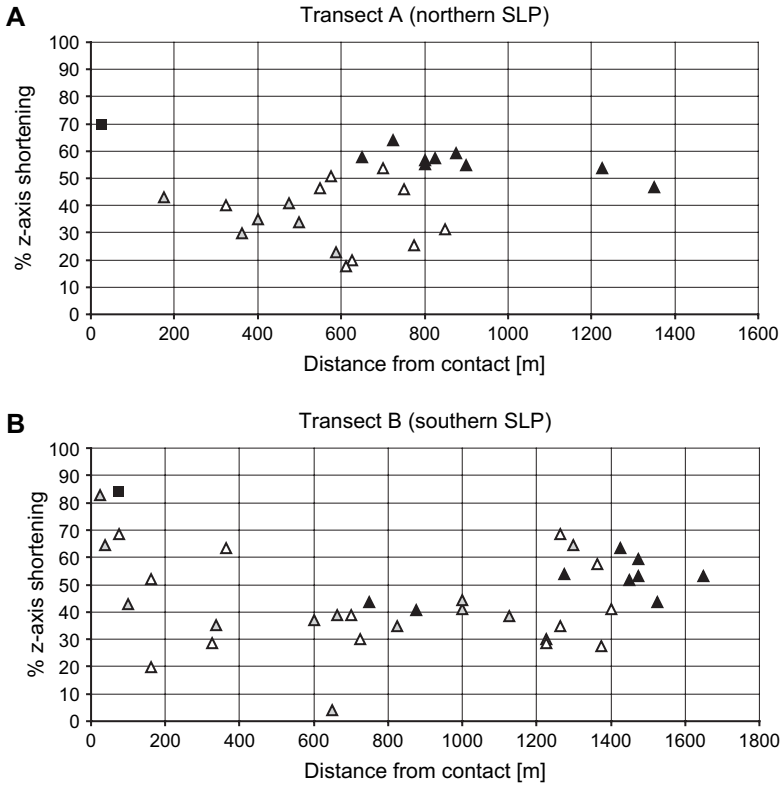

Fig. 7. Spatial distribution of z-axis shortening values along margin-perpendicular transects A and B. White triangles indicate metadacites, gray triangles meta-andesites, and black triangles conglomerates. Black boxes show finite shortening derived from magmatically folded leucocratic dikes (Albertz et al., 2005). Apparent overlap of data from different rock types is due to: (1) projection of data from locations away from transects where contacts are not strictly perpendicular to transects, and (2) lithological layering below the map scale.

void of crystal-plastic strain (Fig. 8H, P). Interstitial phases typically display cuspate geometries and extend along grain boundaries both as continuous films and as small isolated pockets (Fig. 8F–K). Characteristic ''hour-glass'' geometries of cuspate-shaped plagioclase and rounded adjacent quartz crystals (Fig. 8H, I) are strongly reminiscent of pools of crystallized melt (e.g., Garlick and Gromet, 2004) and corroded reactant minerals, respectively (e.g., Sawyer, 2001). Notice the mutually cuspate geometries between plagioclase and K-feldspar in Fig. 8R. The small euhedral feldspar grain above the right arrow may have crystallized from interstitial or grain boundary melt. Line drawings (Fig. 8G, I, K) suggest that the inferred melt pools and films may have formed interconnected melt networks during deformation.

Cuspate geometries in upper amphibolite facies quartzofeldspathic rocks have also been interpreted as the result of diffusion-assisted grain boundary motion involving dissolution, mass transfer and precipitation at quartz-feldspar boundaries (Gower and Simpson, 1992). However, Gower and Simpson (1992) also found evidence for intracrystalline plastic strain by dislocation creep in these rocks, including deformation twins, intracrystalline bending, subgrains, core and mantle textures, irregular and amoeboid grain shapes, and foliation-inclined shear. Furthermore, cuspate portions of boundaries had a much smaller surface area than those gently lobed or straight and cusps were often developed at two-grain contacts (Gower and Simpson, 1992). By comparison, grain boundary cusps in SLP samples typically occur in interstices that are locally connected to inferred crystallized melt films along grain boundaries, they are consistently about the same size as more straight grain margins sections, and evidence for intracrystalline plastic strain is nearly completely lacking (Fig. 8F–R).

In addition to the inferred crystallized melt pockets and films, the following observations are also consistent with the former presence of partial melt. Locally, small myrmekite and quartz subgrains coat feldspar grain boundaries (Fig. 8N, O) and the grain boundaries of some plagioclase minerals are delineated by straight arrays of fluid inclusions (Fig. 8P, Q). Myrmekite may be of magmatic origin (e.g., Hibbard, 1987) or it may form during solid state deformation (e.g., Vernon, 1991). The myrmekite in this study is compatible with either origin and the two processes are not mutually exclusive in this case. However, the fact that myrmekite fringes were found only in samples showing inferred former melt cusps may suggest that myrmekite mimics a partial melt film that has undergone post-crystallization solid state deformation. Likewise, fluid inclusions can form along grain boundaries for a large variety of reasons. Nonetheless, the exclusive occurrence of grain-delimitating fluid inclusion trains near the pluton margin, such as in low energy microstructures (Fig. 8P, Q), may indicate former melt in microtextures that are somewhat more equilibrated than those in the former example (Fig. 8N, O).

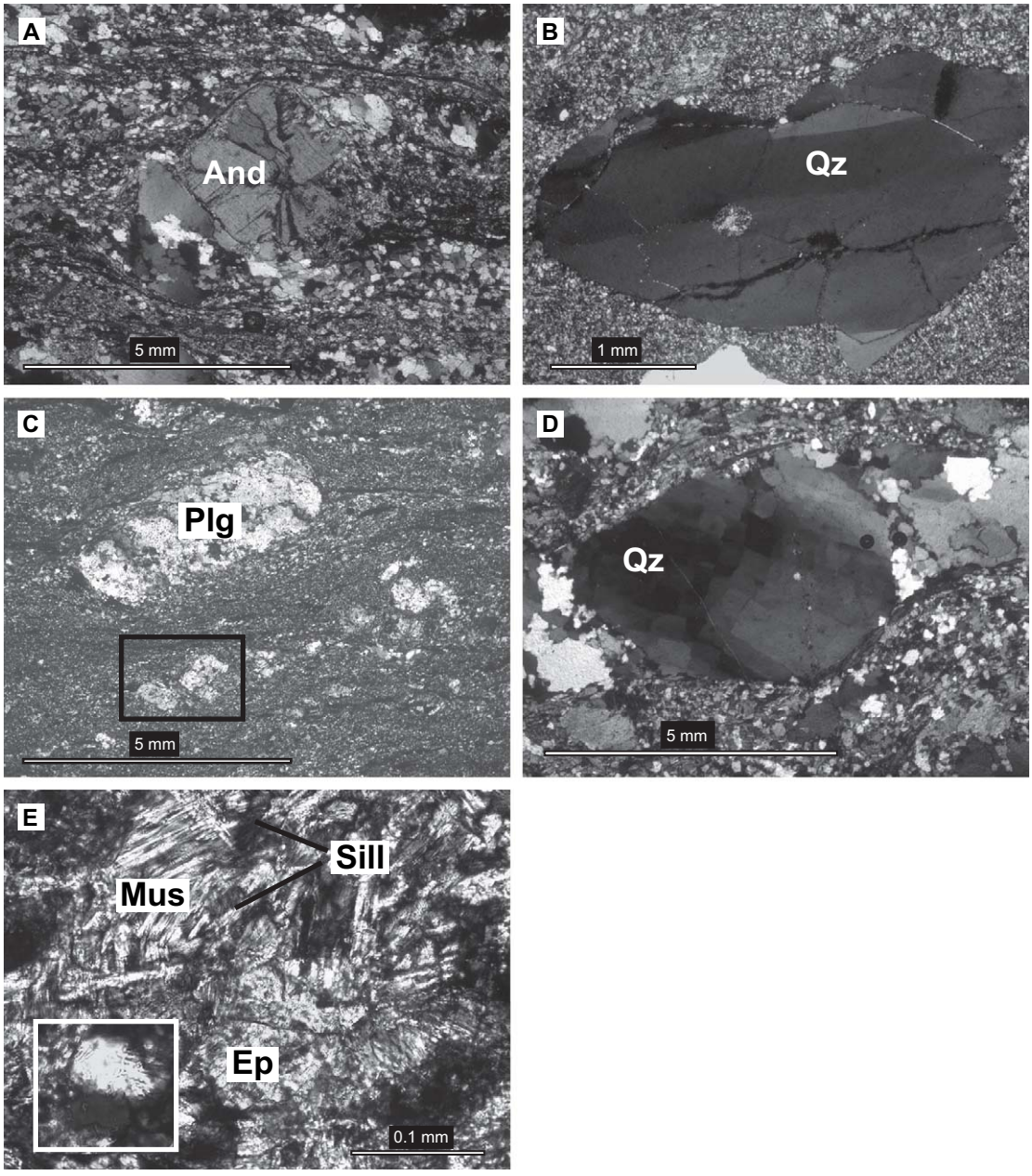

Fig. 8. Photomicrographs of host rocks of the Saddlebag Lake pendant. Abbreviations: And, andalusite; Qz, quartz; Plg, plagioclase; Bio, biotite; Mus, muscovite; Sill, sillimanite; Ep, epidote; Fsp, feldspar; Ksp, K-feldspar. Crossed polarizers in A, B, C, D, E, F, H, J, L, N, P, R. G, I, K, M, O, Q, are line drawings of photomicrographs on the left side showing inferred partial melt. Black indicates quartz or feldspar representing former melt pockets and grain boundary films. Gray depicts myrmekite (O) and fluid inclusion trains (Q). T and V are line drawings of photomicrographs on the left side showing grain-scale fractures. (A) Conglomerate of Cooney Lake with pre- or syn-tectonic andalusite (chiastolite). Foliation wraps around andalusite crystal. Matrix shows rare heterogeneously flattened quartz grains. (B) Rhyolitic ash-flow tuff of Saddlebag Lake. Quartz phenocrysts are marked by patchy to sweeping undulose extinction, deformation bands and/or subgrains. (C) Metaandesite. Plagioclase shows evidence for brittle fracturing. Note the bookshelf-type separation of a phenocryst in the lower half of the photograph (box). Biotite grows in plagioclase cracks and forms coalescing bands. (D) Rhyodacitc ash-flow tuff. Matrix grains are markedly larger than those in (B). Quartz phenocryst shows blocky ''chessboard'' extinction patterns indicating simultaneous basal and prismatic slip in quartz. (E) Horse Canyon sequence. Neocrystallization of fibrous sillimanite and K-feldspar (inset) indicate the second sillimanite isograd. (F) Horse Canyon sequence. Triple-grain interstices are filled with quartz showing weak undulose extinction. Interstices have strong cuspate shaped geometries. (H) Horse Canyon sequence. Notice that none of the grains show evidence for intracrystalline plastic strain. Plagioclase forms conspicuous ''hour-glass'' geometry. Quartz has rounded outlines where in contact with plagioclase and forms straight margins as well as 120° triple junctions in contact with adjacent idiomorphic quartz grains. These observations strongly suggest that the rounded quartz grains are corroded reactant minerals and that the cuspate plagioclase crystallized from interstitial melt pockets. (J) Horse Canyon sequence. Zoned plagioclase with irregular grain margins. (L) Rhyodacitic ash flow tuff displaying intragrain microfractures. Fractures are filled and optically continuous with inferred former melt in matrix. (N) Horse Canyon sequence. Plagioclase and K-feldspar boundaries are fringed by myrmekite and quartz. The fringes are interpreted to represent former grain boundary melt. (P) Horse Canyon sequence. Notice fluid inclusion trains and inferred former melt outlining grain boundaries (see also (Q)). Arrows indicate triple junctions filled with quartz and/or feldspar mimicking former melt pockets. (R) Horse Canyon sequence. Center left shows a geometric arrangement of feldspar grains reminiscent of a four-grain junction. Four-grain junctions form during granular flow when grains are shuffled and switch neighbors. Note the mutually cuspate geometries between plagioclase and K-feldspar (arrows). Small euhedral feldspar above right arrow may have crystallized in melt pocket. (S) Rhyolitic ash-flow tuff of Saddlebag Lake at ca. 1 km distance to pluton margin. The original crystal shape of quartz is roughly preserved. Matrix includes K-feldspar and plagioclase. (U) Rhyodacitic ash-flow tuff at the pluton margin. Quartz phenocrysts are elongated by fracture-related mechanical abrasion. Matrix includes K-feldspar and plagioclase.

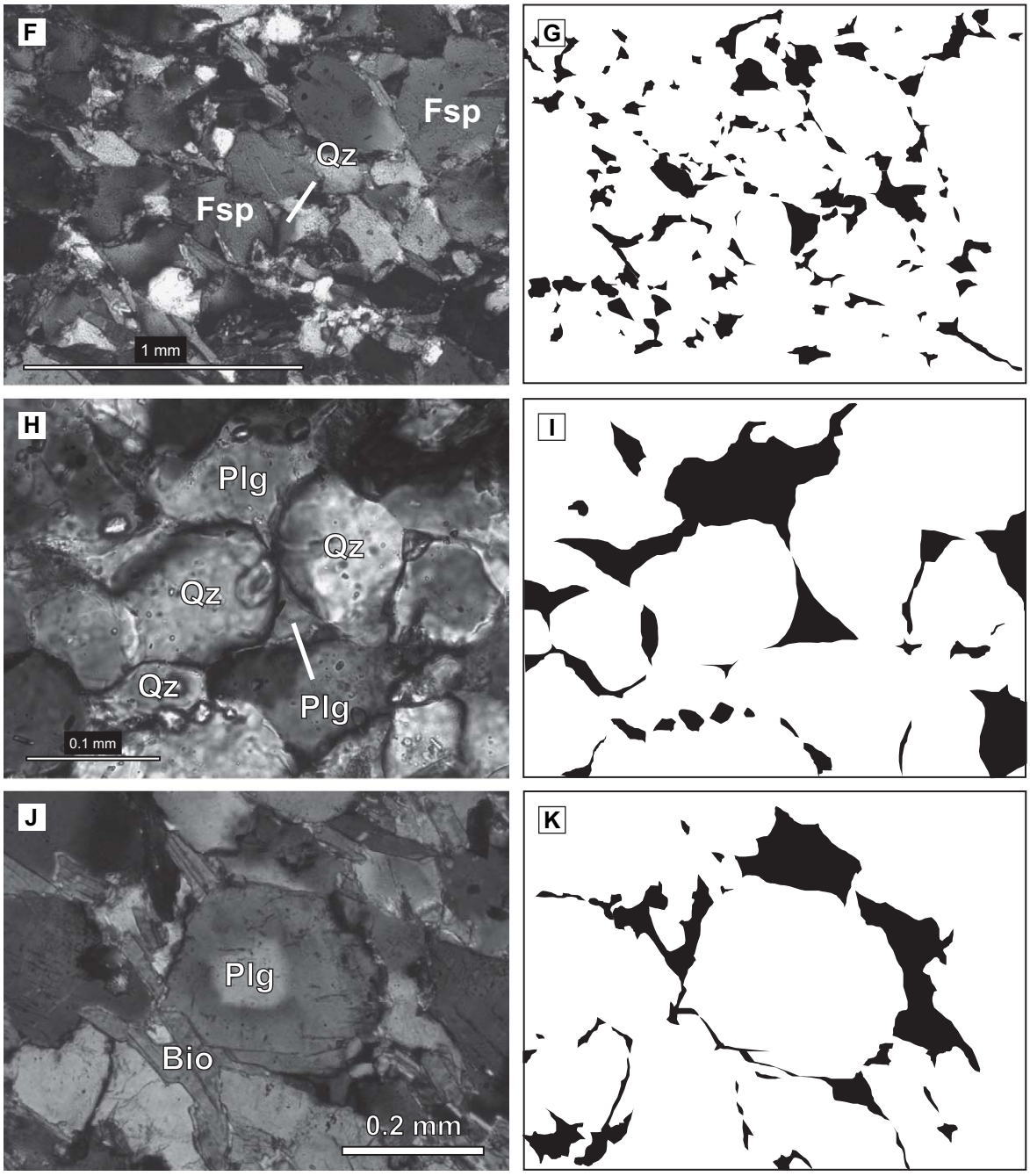

Fig. 8 (*continued*)

In addition, microfracturing is common near the pluton margin. Fig. 8L depicts intragrain cracking of plagioclase. Quartz filling the crack is connected and optically continuous with matrix cusps. Deposition from hydrothermal solution cannot be ruled out but fractures do not extend into adjacent grains suggesting cracking during the presence of intergranular melt. Hence, on the basis of mineral parageneses, melt-bearing microstructures, and outcrop-scale migmatization (Fig. 4), the deformation temperature near the pluton margin is constrained to at least ca. 650–750 °C (Spear, 1993).

The transition from high-temperature to melt-bearing microstructures is marked by an increasing importance of intragrain cracking. Though cracks occur well beyond the pluton margin, for example at a distance of ca. 1 km to the contact, subhedral to euhedral quartz phenocrysts are relatively intact and preserve their original shape (Fig. 8S, T). By comparison, samples marking the transition to the zone of melt-bearing microstructures within ca. 100 m to the pluton margin show much more intense fracture-related damage (Fig. 8U, V). This cracking is typically concentrated along the margins of the phenocrysts and effectively leads to mechanical abrasion of larger grains and generation of smaller fragments. Fig. 8U and V illustrate that the newly generated small grain fragments derived from larger quartz phenocrysts literally are smeared

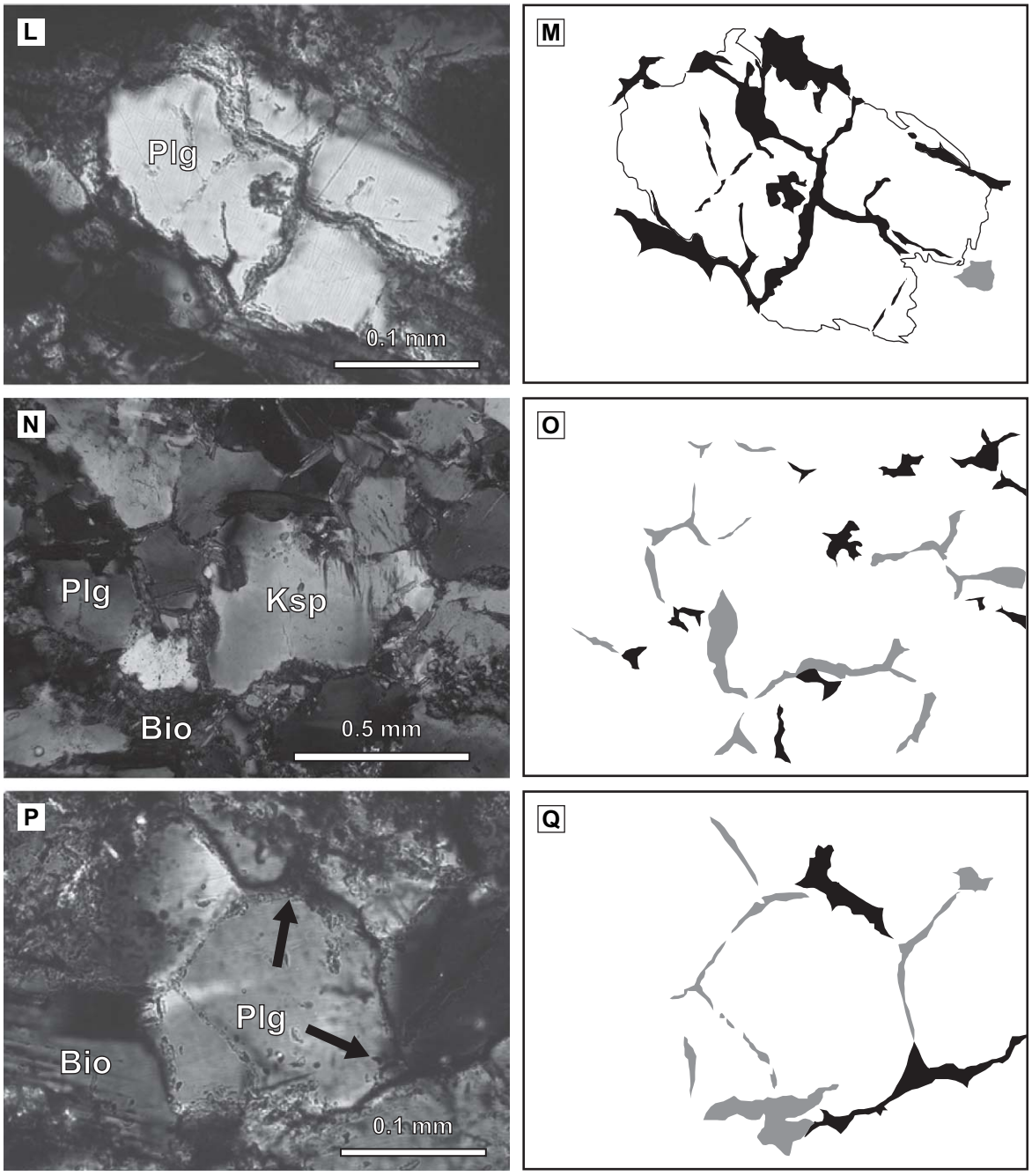

Fig. 8 (*continued*)

out along the grains, resulting in overall grain elongation and a noticeable increase in foliation intensity in the field.

5. Interpretation of microstructures

The microstructural observations suggest that temperature increased from ca. 350–400 °C at a distance of ca. 300–900 m to the pluton and beyond, to more than ca. 620–650 °C up to ca. 100 m distance to the pluton, and finally to ca. 650–750 °C closest to the margin. Along with this temperature increase the dominant deformation mechanisms adjusted correspondingly.

5.1. Deformation mechanisms

Hirth and Tullis (1992) experimentally determined three dislocation creep regimes in quartz aggregates. With progressively increasing laboratory temperature and/or decreasing strain rate, diagnostic microstructures developed. Despite lower temperatures and strain rates in nature, several works correlated these dislocation creep regimes with natural microstructures (e.g., Dunlap et al., 1997; Stöckhert et al., 1999; Zulauf, 2001). In a recent study, Stipp et al. (2002) systematically examined the complete range of quartz recrystallization microstructures in a single tectonometamorphic setting. These authors analyzed

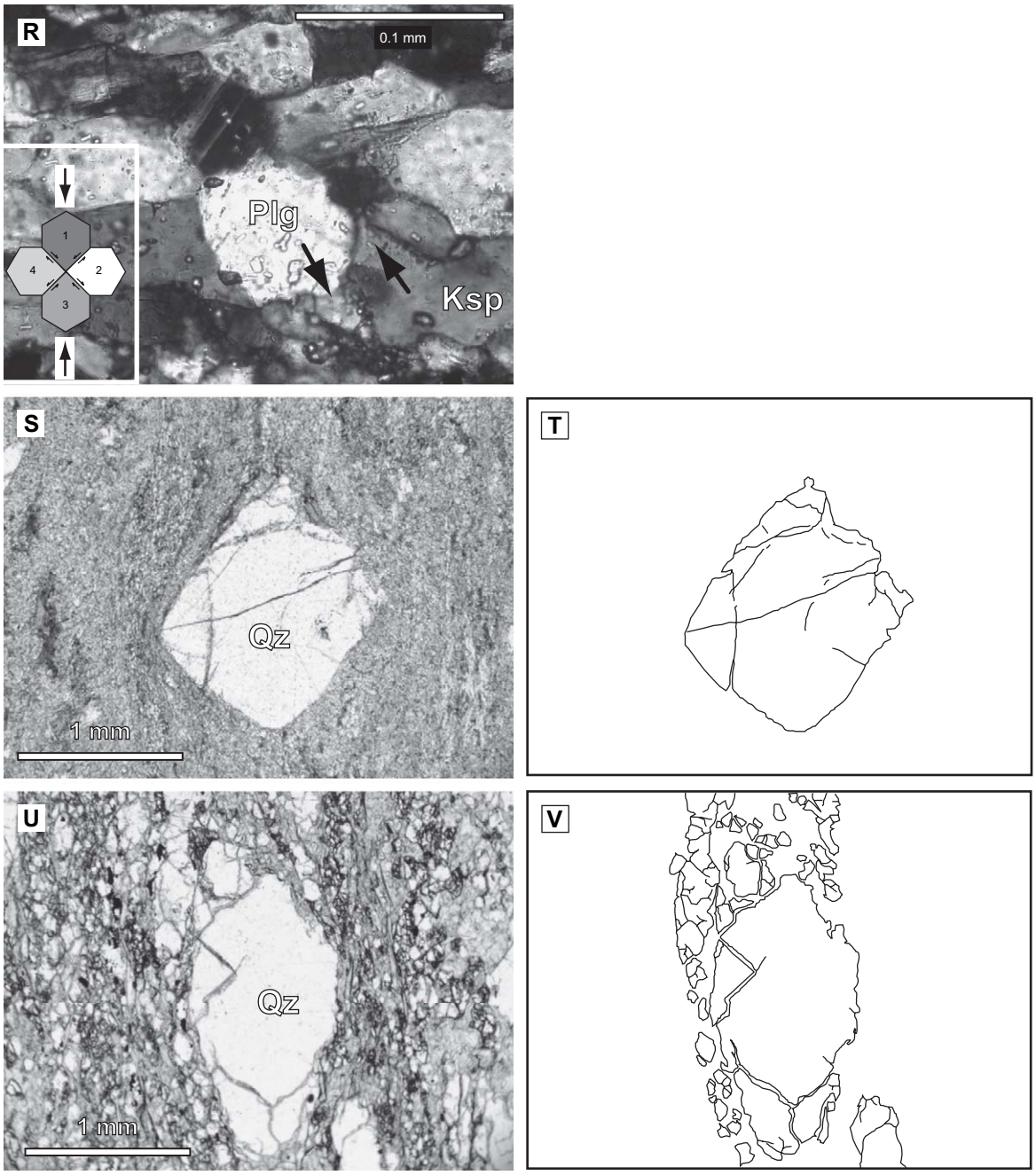

Fig. 8 (*continued*)

microstructures in deformed quartz veins in the contact aureole of the Adamello pluton and independently estimated temperatures utilizing metamorphic phase assemblages.

Based on the strong resemblance of the quartz microstructures described above (Section 4) to those described in Stipp et al. (2002) and those generated experimentally (Hirth and Tullis, 1992), it is inferred that analogous transitions between dislocation creep regimes occurred in the SLP. Weak elongation of original grains, locally bulging grain boundaries, patchy to sweeping undulose extinction, and deformation bands and/or incipient subgrains (Fig. 8A, B), strongly resemble those observed in dislocation creep regimes 1 and 2 generated experimentally by Hirth and Tullis (1992). As regards the Adamello aureole, Stipp et al. (2002) concluded that bulging recrystallization (dislocation creep regime 1 of Hirth and Tullis, 1992) was dominant between ca. 280 and 400 °C and that subgrain rotation recrystallization (dislocation creep regimes 2 and 3 of Hirth and Tullis, 1992) occurred between ca. 400 and 500 °C. In the SLP, the highly irregular and seriate-interlobate grain margins closer to the pluton margin indicate grain boundary migration recrystallization (Passchier and Trouw, 2005). Grain boundary migration recrystallization is diagnostic of experimental dislocation creep regime 3 observed with increased laboratory temperatures and decreased

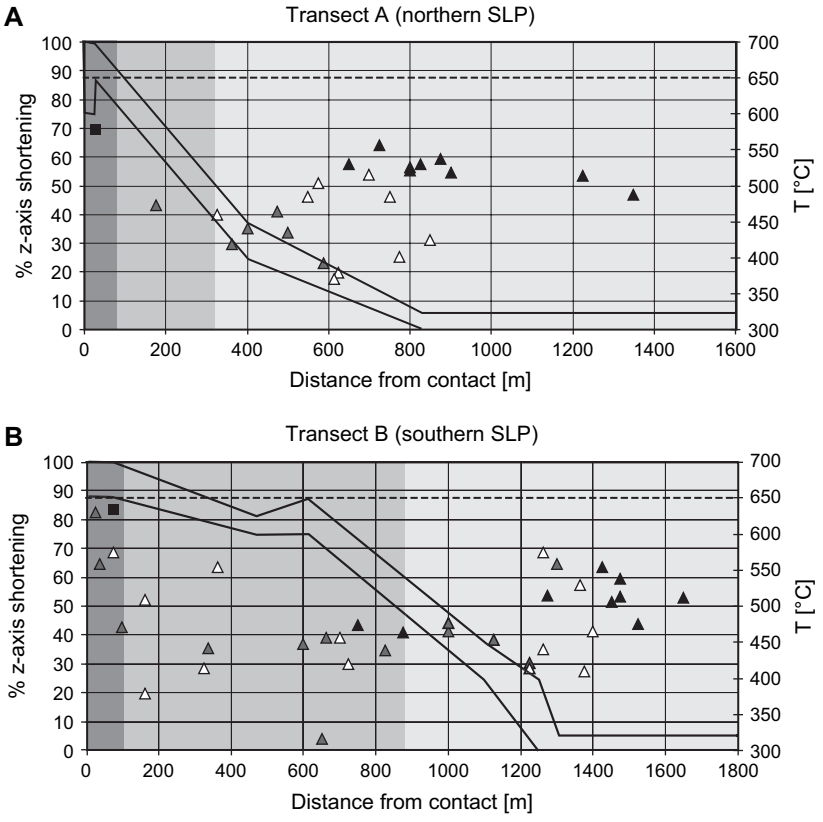

Fig. 9. Diagrams showing as a function of position in the SLP: values of *z*-axis shortening (white triangles indicate metadacites, gray triangles metaandesites, and black triangles conglomerates; black boxes show finite shortening derived from magmatically folded leucocratic dikes; Albertz et al. (2005)), temperature constraints obtained from diagnostic microstructures and metamorphic phase assemblages (lower and upper solid black lines depict temperature brackets; dotted horizontal line indicates melting temperature), and dominant deformation mechanisms (dark gray shading shows melt-assisted granular flow, gray high-temperature dislocation creep, and light gray low-temperature dislocation creep). (A) Northern transect. (B) Southern transect.

strain rates compared to dislocation regimes 1 and 2 (Hirth and Tullis, 1992). Stipp et al. (2002) found that the transition to grain boundary migration recrystallization in the Adamello aureole occurred at ca. 500 °C. Likewise, grain boundary migration recrystallization in the SLP was associated with increased temperature as indicated by the presence of highly irregular grain margins and ''chessboard'' patterns in quartz phenocrysts (Fig. 8D). Hence, with increasing temperature toward the pluton margin, low-temperature dislocation creep (ca. 350–400 °C) was replaced by high-temperature dislocation creep (ca. 500 to ≥620–650 °C).

Despite lacking microstructural evidence for crystal-plastic strain within ca. 100 m to the pluton margin, the host rocks have experienced large amounts of shortening (Section 3; Albertz et al., 2005). Strain-free grains in highly deformed rocks may provide indirect evidence for granular flow (e.g., Fliervoet et al., 1997; Rutter et al., 1994; Berger and Rosenberg, 2003). Granular flow is further suggested by the presence of approximately equant grains arranged in four-grain junctions (box in Fig. 8R). In view of the possible presence of a small grain boundary segment between grains 2 and 4 (Fig. 8R), this configuration might indicate an incipient or passing intermediate state of a transient neighbor-switching event whereby grains are shuffled during large relative movement of grains (Poirier, 1985).

In a previous study, we calculated cooling times of magmatically folded dikes to estimate the rates associated with folding (Albertz et al., 2005). The results included strain rates several orders of magnitudes larger than those typical for dislocation creep, suggesting that ''faster'' processes, such as melt-assisted granular flow, must have operated to accommodate host rock shortening. Outcrop-scale migmatization, the inferred presence of melt pools in interstices and along grain boundaries, as well as myrmekite fringes (Section 4; Albertz et al., 2005) strongly support that proximal deformation in the SLP was accommodated by melt-assisted granular flow. This interpretation explains the conspicuous lack of appreciable intracrystalline plastic strain despite large amounts of finite shortening observed at the outcrop scale.

5.2. Role of microfracturing

Key observations suggest that microfracturing may have played a critical role in triggering the transition from high-temperature dislocation creep to melt-assisted granular flow. Fig. 8S–V illustrates efficient grain size reduction by intragrain cracking, reducing grain size to a level possibly more favorable for granular flow to operate as the dominant deformation mechanism. Laboratory experiments give hints as to what might cause cracking during partial melting.

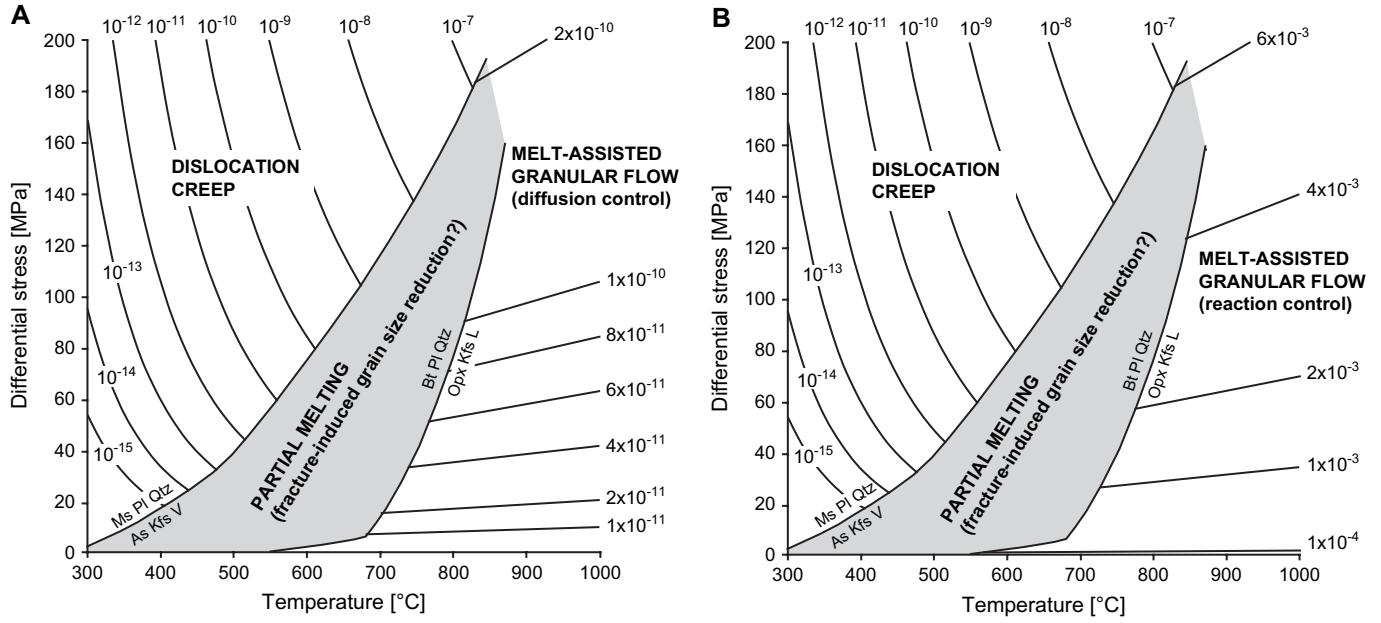

Fig. 10. Modified deformation mechanism maps showing the melt-induced transition from dislocation creep to granular flow. (A) Melt-assisted granular flow with diffusion as rate-limiting process. (B) Same as (A), but with reaction control. Melting reactions from Spear (1993). Parameters from Hirth et al. (2001) and Paterson (2001). Contour lines indicate strain rates in s^{-1}.

Rushmer (1995) deformed partially molten amphibolite using a hydrous phase breakdown reaction. The results indicated a transition from dominantly crystal-plastic deformation to fracturing to viscous flow with increasing melt fraction. Subsequent experiments (Rushmer, 2001) on volume changes associated with dehydration melting of muscovite + biotite-bearing pelites and biotite + plagioclase + quartz gneiss samples showed that the muscovite-bearing samples developed melt-filled microfractures (see also Connolly et al., 1997), while the biotite gneiss samples did not. These experiments suggested that volume change alone may not be the only driving force for cracking and melt segregation in biotite-only-bearing assemblages and that external deformation may be required. Clearly, additional work is desirable to evaluate the importance of cracking with regards to triggering melt-assisted granular flow in a quantitative sense.

6. Discussion

6.1. Finite strain

The data presented in Section 3 represent the total finite strain accumulated in the Piute Meadow pendant (PMP) and Saddlebag Lake pendant (SLP). Because construction of the Tuolumne Intrusive Suite (TIS) presumably was accommodated by material displacement in front of the moving magma (e.g., Paterson and Fowler, 1993), it is likely that at least some of the finite strain in the SLP resulted from emplacement-related deformation. A lacking strain gradient in the PMP, however, largely dismisses material displacement by ductile processes at the northern end of the TIS. Hence, two questions arise: (1) what type of regional strain regime are the data consistent with; and (2) can we separate the contributions from emplacement-related and regional strain?

6.1.1. Regional strain

Several scenarios have been advanced to explain the tectonic evolution of the Sierra Nevada. Tobisch et al. (1986, 1993) suggested that the Sierra Nevada magmatic arc was dominated by extensional tectonics, but the authors subsequently proposed that strain fields varied from extensional to neutral to contractional, ultimately related to the degree of obliquity of the convergence between the North America and Farallon plates (Tobisch et al., 1995). Greene and Schweickert (1995) invoked a model of dextral transpression coexisting with emplacement of granitic plutons (Sharp et al., 2000). In addition, oblique convergence may have resulted in syn-magmatic strike-slip partitioning during the Late Cretaceous (Tikoff and de Saint Blanquat, 1997).

Three key observations suggest that the strain data of this study are consistent with regional contraction and/or weakly dextral transpression: (1) in the PMP, stretching lineations plunge subvertically and there is evidence for vertical shear only; (2) in the SLP, oblique shear is indicated by a domain of moderately SE-plunging lineations and slightly prevailing dextral shear senses, although horizontal kinematic indicators are rare and variable; and (3) strain ellipsoid shapes in the PMP and SLP indicate plane strain deformation. It remains unclear whether the regional strain regime was dominated by contraction or transpression, and to what degree deformation was partitioned. The complete lack of horizontal shear kinematics in the PMP, as well as variable and only rare dextral kinematics in the SLP, makes it difficult to support regionally continuous strike-slip displacement, such as on the proposed Sierra Crest shear zone system (Tikoff and de Saint Blanquat,

1997). Based on predicted plane strain geometries in high-''press'' transpression zones (Robin and Cruden, 1994), however, it appears that the data are consistent with close to ''head-on'' convergence between the North America and Farallon plates during the Late Cretaceous. Small variation in the convergence angle could have resulted in a switch from contraction to transpression and vice versa.

6.1.2. Emplacement-related strain

Pluton emplacement in the Sierra Nevada was often associated with lateral expansion, resulting in flattening type strains in contact aureoles (e.g., Tobisch et al., 1986, 1993; McNulty et al., 1996, 2000). Strain ellipsoid shapes significantly more oblate than those typical of regional deformation have also been found in aureoles elsewhere (Bateman, 1985; John and Blundy, 1993). This is consistent with analog models of diapirism predicting flattening strains in wall rocks (e.g., Cruden, 1988). In addition, magma chamber expansion often deforms older peripheral plutonic units (e.g., Johnson et al., 2003) and expansion can deflect markers with regionally consistent strikes (e.g., contacts, foliations, faults) in aureoles (Paterson et al., 1994; Albertz et al., 2001), particularly if they are highly discordant, such as in the PMP (Fig. 2B).

However, the following observations suggest that lateral expansion entailing wall rock flattening is not applicable to the Piute Meadow pendant (PMP) and Saddlebag Lake pendant (SLP): (1) the strain data consistently indicate plane strain deformation; (2) a ductile deformation aureole does not exist in the PMP; (3) most sections of the pluton margin do not show marker deflection; and (4) strain ellipsoids indicate a shortening direction parallel to the ca. NE-striking pluton margin (Fig. 2A).

Alternative hypotheses are that emplacement-related material displacement involved plane strain deformation inseparable from regional strain on the basis of strain ellipsoid shapes, or that large-scale material removal, for example by stoping and assimilation, accommodated construction of the TIS. It is also possible that a flattened aureole once existed but was removed.

6.1.3. Removal of inner aureoles

Exposures of highly irregular and discordant pluton margins suggest that thermal cracking, stoping, and by inference assimilation may occur during pluton emplacement (e.g., Clarke et al., 1998), and that aureoles are potentially subject to loss of their inner portions (Buddington, 1959; Paterson and Vernon, 1995). For example, stoped blocks in the Beer Creek Pluton in the White Mountains, California, show structures characteristic of the deformation aureole (Albertz et al., 2000), supporting removal of emplacement-related, ductilely deformed portions of the aureole. In addition, numerical modeling studies indicate that when stoping occurs, the aureole rocks immediately adjacent to the pluton margin are progressively less strained (Gerbi et al., 2004), and that the inner portions, including evidence for emplacement-related strain rates (and thus finite strain), may even be completely lost (Albertz and Johnson, 2006).

Stepped, discordant and highly irregular contact relationships in the Piute Meadow pendant (PMP, Fig. 2A) and Saddlebag pendant (SLP, Fig. 3A), as well as variously sized, isolated host rock blocks in the SLP suggest that stoping occurred at the emplacement level. The absence of large amounts of stoped blocks may in fact stress the efficiency of stoping (Paterson and Okaya, 1999; Pignotta et al., 2001; Yoshinobu et al., 2003), although this can at best be considered circumstantial evidence. A more convincing argument for stoping in the SLP is that a portion of the inner aureole, including stratigraphy and the corresponding finite strains, is missing. Notice that rocks of the Horse Canyon sequence as well as older TIS units are truncated at a high angle to strike by Cathedral Peak granodiorite (Fig. 3A). As a result, z-axis shortening at the margin in transect A is 70% (Fig. 7A) whereas 85% shortening was preserved in transect B (Fig. 7B). Also notice that the width of the domain of high-temperature microstructures along transect A is only ca. 1/3 the equivalent width in transect B (Fig. 9). While these observations strongly support stoping, complete removal of ductile aureole strain is unlikely. If this was the case, the strain gradient in the SLP would not have been preserved. It remains unknown whether flattening strain ever existed in the PMP and SLP. The strain gradient in the SLP could have formed by combined emplacement-related and regional host rock shortening or by regional strain alone.

6.2. Relationships between finite strain and microstructure in the SLP (Saddlebag Lake pendant)

The transition between low- and high-temperature dislocation creep is not associated with noticeable changes in finite strain (Fig. 9). Neither strain transect indicates systematic gradients in those portions of the SLP showing dislocation creep microstructures (Fig. 9). Increased rates of grain boundary migration with higher temperatures (Hirth and Tullis, 1992) ultimately should result in higher finite strains because this would allow the affected rocks to deform faster in a given amount of time. However, a numerical examination of dislocation creep rates using a flow law points out that, particularly at temperatures of 500 °C and higher, rates are rather insensitive to temperature changes (Albertz and Johnson, 2006). These considerations imply that transitions between dislocation creep regimes may not prompt significant strength reduction.

In contrast, an abrupt increase in finite strain coincides with the transition from high-temperature dislocation creep to melt-assisted granular flow. Within ca. 100 m to the pluton margin, transects A and B (Fig. 9) show that finite strains increase abruptly from ca. 43% (average regional shortening) to ca. 70 and 85%, respectively. The strain increase correlates with the first occurrence of melt-bearing microstructures, suggesting that melt-assisted granular flow is an efficient mechanism of rheological weakening in pluton environments.

Rosenberg and Handy (2005) argued that a previously unrecognized, but even more important strength drop occurs at melt fractions much lower than originally proposed (e.g., Arzi, 1978; van der Molen and Paterson, 1979). The authors

illustrated a drastic decrease in effective viscosity between the solidus and $\Phi = 0.06$ to 0.07 corresponding to a loss of ca. 90% of the sample strength. In terms of possible mechanisms of weakening, Rosenberg and Handy (2005) suggested that localized, inter- and intragranular microcracking, as well as some rigid-body rotation of grains and grain aggregates accommodated by frictional sliding and movement along incipient melt pockets facilitated deformation. An association of microfractures and partial melting has been corroborated in other experiments (e.g., Rushmer, 1995; Connolly et al., 1997; Rushmer, 2001). With regards to extrapolating the results to natural deformation, however, Rosenberg and Handy (2005) alerted to some difficulty because the dominant deformation mechanism in the experiments was cataclastic flow, whereas natural rocks undergoing partial melting appear to deform by viscous flow (Rosenberg, 2001). In addition, the experimental data were obtained for finite strains of merely 1–6% shortening, but the present study indicates that shortening in natural aureoles can amount to at least 85%.

This study suggests that microfracturing in partially melted rocks may lead to mechanical grain size reduction (Fig. 8S–V) thus creating better conditions for melt-assisted granular flow, favored by small grain size (e.g., Paterson, 2001). During progressive deformation to large finite strains, however, evidence for fracture-related grain size reduction may be obliterated because large relative movement and rearrangement of grains during granular flow can obscure the microstructure. Furthermore, as soon as an interconnected melt network is established, cracking may become much less important because melt can be channeled into melt conduits and eventually escape, preventing further build-up of melt pressure. Because the foregoing discussion implies that grain size reduction may have preceded melt-assisted granular flow, microfracturing might be, at least in some cases, a condition for melt-assisted granular flow. Thus it may in fact not be surprising that low strain deformation experiments on partially melted rocks show ample evidence for cataclastic flow but natural observations do not.

6.3. Implications for the rheology of partially melted rocks

Lastly, an attempt is made to semi-quantitatively illustrate the effect of rheological weakening in partially melted rocks with low melt fractions. Paterson (2001) devised a flow law for the deformation of partially melted rocks which is used here together with a quartz dislocation creep flow law to construct modified deformation mechanism maps. Conventional deformation mechanism maps are produced by equating the experimentally determined constitutive equations and plotting the boundary at which the strain rates are equal for a range of pressures and temperatures (e.g., Stocker and Ashby, 1973). However, applying this procedure to find the strain rate contours at the boundary between dislocation creep and melt-assisted granular flow in nature would require unrealistically high temperatures for dislocation creep to satisfy the requirement of equal strain rates ($>>1000\,^{\circ}C$ for ca. 100 MPa differential stress for reaction-limited granular flow (estimated from parameters in Paterson, 2001). More importantly, the transition from dislocation creep to melt-assisted granular flow in partially melted rocks in nature is not caused by increasing temperature alone but primarily by the introduction of partial melt to the system.

Paterson's (2001) granular flow theory includes three flow laws accounting for melt viscosity, diffusion, and melting reaction as rate-limiting factors associated with interference of grains moving past each other. We consider a melt fraction of $\Phi = 0.05$, grain size = 0.1 mm, and combine the diffusion- and reaction-controlled end members of melt-assisted granular flow for open systems (Paterson, 2001) with Hirth et al.'s (2001) calibrated quartz flow law. The viscosity-controlled case is omitted, because in it, strain rate does not depend on pressure and temperature (it predicts strain rates one order magnitude larger than the reaction-controlled case). The modified deformation mechanism map for the diffusion-controlled case (Fig. 10A) shows that the transition from dislocation creep to melt-induced granular flow in quartz-rich rocks, for example at 10–20 MPa differential stress, is associated with a change in strain rate from ca. $10^{-14\pm1}\ s^{-1}$ to ca. $10^{-11}\ s^{-1}$. For the reaction-controlled case, the corresponding strain rate changes from ca. $10^{-14\pm1}\ s^{-1}$ to ca. 10^{-4} to $10^{-3}\ s^{-1}$. Given the uncertainty of the location of the melting reactions and the granular flow theory itself (Paterson, 2001), the relationships in Fig. 15 are meant to illustrate order-of-magnitude changes associated with a melt-induced transition from dominantly dislocation creep to granular flow and should not be taken at face value.

Despite, the modified deformation mechanism maps illustrate that a melt-induced switch from dislocation creep to granular flow in nature could be associated with at least 2 orders of magnitude increase in strain rate. To demonstrate the effect of rheological weakening we can use a simple relationship between effective viscosity, μ_{eff}, differential stress, σ (e.g., tectonic stress), and strain rate, $\dot{\epsilon}$(e.g., Poirier, 1985):

$$\mu_{eff} = \sigma/\dot{\epsilon} \tag{1}$$

For $\sigma = 10$ MPa, and a change in $\dot{\epsilon}$ from $10^{-14\pm1}$ to $10^{-11}\ s^{-1}$, μ_{eff} would drop from $10^{21\pm1}$ to $10^{18\pm1}$ Pa s.

As a conjecture, one can think about how fracture-induced grain size reduction (Section 5.2) might tie into the modified deformation mechanism maps. If microfractures were genetically related to positive volume changes during partial melting (Rushmer, 1995, 2001; Connolly et al., 1997), then it would seem reasonable to assume that fracture-induced grain size reduction should occupy a position in the modified deformation mechanism maps between dislocation creep and melt-assisted granular flow (Fig. 10).

6.4. Constraints for emplacement models of the Tuolumne Intrusive Suite (TIS)

Although the primary motivation of this study was to examine the contributions from melt-absent and melt-present deformation mechanisms to the total finite strain, the results can be integrated with emplacement models to further constrain the

evolution of the TIS. Any emplacement model for the TIS should account for the following five key aspects: (1) highly discordant contact relationships as well as lack of a ductile aureole and marker deflection in the Piute Meadow pendant (PMP), (2) abruptly increasing strain intensities towards the pluton and constant strain ellipsoid geometry in the Saddlebag Lake pendant (SLP), (3) removal of stratigraphy and finite strain in the SLP, (4) subvertical foliations and lineations in the PMP and SLP as well as locally moderately plunging stretching lineations in the SLP, and (5) magmatic foliations with margin-parallel and regional NNW strikes.

Tikoff et al. (2005, and therein) proposed syn-emplacement dextral displacement on the Cascade Lake shear zone along the eastern TIS margin. Based on data collected in an area extending more or less across strike only and tracing the pluton margin for no more than ca. 1 km (Fig. 1C in Tikoff et al., 2005; Fig. 3 in Davis, 1996), the authors stated that the Cascade Lake shear zone is structurally continuous with the Gem Lake and Rosy Finch shear zones to the south and together form the Sierra Crest shear zone system. However, generally rare kinematic indicators along the ca. 10 km long continuous exposure in the (SLP) show domains of dextral, sinistral, as well as pure shear kinematics (Albertz and Paterson, 2002) rather than consistent dextral sense of shear. Furthermore, horizontal kinematics and/or mylonites in support of a continuous shear zone are lacking along the projected northward and southward continuations.

Another recently proposed emplacement model for the TIS entails incremental magma emplacement by progressive amalgamation of multiple subvertical sheets without the need for large chambers ever to exist (Glazner et al., 2004). The authors relied on post-emplacement static recrystallization to explain the lack of internal contacts. However, well-preserved microstructures in host rocks (Section 4) as well as granitoids of the TIS (Albertz et al., 2005) are not consistent with widespread static recrystallization. Furthermore, dikes in the SLP are limited to a ca. 2 km long section only (Fig. 3A) and in the PMP, dikes are very rare although here, on mechanical grounds, preexisting anisotropies should have provided favorable sites for dike propagation. In addition, magmatic foliations consistently crosscut contacts between plutonic units and swing into parallelism with the northern TIS margin (Fig. 2B).

The data at hand suggest that stoping, assimilation, and large-scale vertical material transfer through a narrow aureole may have played primary roles during emplacement of the TIS.

7. Conclusions

Quantitative finite strain analyses in the northern (Piute Meadow pendant (PMP)) and eastern (Saddlebag Lake pendant (SLP)) host rock pendants of the Tuolumne Intrusive Suite (TIS) indicate that finite strains abruptly increase from ca. 43% to 70–85% within ca. 100 m of the pluton margin in the SLP. The strain increase coincides with a switch from high-temperature dislocation creep to melt-assisted granular flow possibly induced by fracturing. A comparison of strain rates derived from flow laws of dislocation creep in quartz aggregates and melt-assisted granular flow implies that the transition between the two rheological domains may involve changes in effective viscosity spanning at least two orders of magnitude. The results are consistent with experimental work and confirm that melt-assisted granular flow is an efficient mechanism conducive of rheological weakening in nature.

Highly discordant cross-cutting relationships in both host rock pendants, complete lack of ductile pluton-related strain in the PMP, and a steep strain gradient in the SLP suggest that stoping and by inference assimilation as well as vertical material displacement in a narrow aureole was of primary importance during emplacement of the TIS. Evidence for obscuring of internal contacts by post-emplacement static recrystallization in support of incremental dike assembly is lacking. Plane strain fabric ellipsoids, predominantly vertical stretching lineations, and locally moderately SE-plunging lineations are consistent with contractional regional strain and/or weakly dextral transpression.

Acknowledgements

This work was funded by a USC Graduate Student Research Grant, a Geological Society of America Grant, and a DAAD (Deutscher Akademischer Austauschdienst) doctoral fellowship. Partial funding was also available from NSF grant number EAR-0073943 (awarded to Scott Paterson). I thank Scott Paterson, Jean Morrison, Robert Miller, Greg Davis, Chris Carlson, and Demetrius Pohl for scientific discussions. The fieldwork in remote areas of the high Sierra Nevada would not have been possible without the assistance and company of Mecki Rieber, Helge Alsleben, Tim Weber, and Dominique Richard. The Yosemite National Park Service, Bart Cranney (Leavitt Meadows Pack Station), and in particular Tim Forsell (Forest Service Ranger at Piute Cabin) are thanked for logistical assistance. King Huber kindly provided copies of Clyde Wahrhaftig's field maps. Informal reviews by Scott Paterson and Claudio Rosenberg improved an early draft of this manuscript. Jörn Kruhl and Tracy Rushmer are thanked for thorough and thoughtful formal reviews.

References

Ague, J.J., Brimhall, G.H., 1988. Magmatic arc symmetry and distribution of anomalous plutonic belts in the batholiths of California: effects of assimilation, crustal thickness, and depth of crystallization. Geological Society of America Bulletin 100, 912–927.

Ague, J.J., 1991. Evidence for major mass transfer and volume strain during regional metamorphism of pelites. Geology 19, 855–858.

Albertz, M., Paterson, S.R., 2002. Three-dimensional pure shear during transpression: the effect of Cretaceous plutonism on regional strain fields in the Sierra Nevada batholith, California. Abstracts with Programs - Geological Society of America 34, 328.

Albertz, M., Paterson, S.R., Okaya, D., 2005. Fast strain rates during pluton emplacement: magmatically folded leucocratic dikes in aureoles of the Mount Stuart Batholith, Washington and the Tuolumne Intrusive Suite, California. Geological Society of America Bulletin 117, 450–465.

Albertz, M., Paterson, S.R., Miller, R.B., Piontek Matzel, J., Okaya, D., 2001. Mt. Stuart Batholith, Washington: constraints on emplacement-related strain rates from thermo mechanical modeling and deflection of regional markers. EOS Transactions, AGU Spring Meeting Supplement, Abstract T52A-04.

Albertz, M., Wetmore, P.H., Pignotta, G.S., Potter, M.E., Andreasson, G., Paterson, S.R., 2000. How do magma chamber-host rock systems evolve through time? Abstracts with Programs - Geological Society of America 32, 1.

Albertz, M., Johnson, S.E., 2006. Modeling dislocation creep as a near-field material transfer process during spherical pluton expansion: implications for strain rates and their preservation in pluton aureoles. Journal of Structural Geology 28, 253–267.

Aoya, M., Wallis, S.R., Terada, K., Lee, J., Kawakami, T., Wang, Y., Heizler, M., 2005. North-south extension in the Tibetan crust triggered by granite emplacement. Geology 33, 853–856.

Arzi, A.A., 1978. Critical phenomena in the rheology of partially melted rocks. Tectonophysics 44, 173–184.

Bateman, P.C., 1992. Plutonism in the central part of the Sierra Nevada Batholith, California. US Geological Survey Professional Paper 1483, 186.

Bateman, P.C., Chappell, B.W., 1979. Crystallization, fractionation, and solidification of the Tuolumne intrusive series, Yosemite National Park, California. Geological Society of America Bulletin 90, 465–482.

Bateman, R., 1985. Aureole deformation by flattening around a diapir during in situ ballooning: the Cannibal Creek granite. Journal of Geology 93, 293–310.

Beaumont, C., Jamieson, R.A., Nguyen, M.H., Medvedev, S., 2004. Crustal channel flows: 1. Numerical models with applications to the tectonics of the Himalayan-Tibetan orogen. Journal of Geophysical Research 109, B06406, doi:10.1029/2003JB002809.

Beaumont, C., Jamieson, R.A., Nguyen, M.H., Lee, B., 2001. Himalayan tectonics explained by extrusion of a low-viscosity crustal channel coupled to focused surface denudation. Nature 414, 738–742.

Berger, A., Rosenberg, C.L., 2003. Preservation of chemical residue-melt equilibria in natural anatexite: the effects of deformation and rapid cooling. Contributions to Mineralogy and Petrology 144, 416–427.

Bohlen, S.R., Montana, A., Kerrick, D.M., 1991. Precise determinations of the equilibria kyanite sillimanite and kyanite andalusite and a revised triple point for Al2SiO5 polymorphs. American Mineralogist 76, 677–680.

Buddington, A.F., 1959. Granite emplacement with special reference to North America. Geological Society of America Bulletin 70, 671–747.

Clarke, D.B., Henry, A.S., White, M.A., 1998. Exploding xenoliths and the absence of ''elephants' graveyards'' in granite batholiths. Journal of Structural Geology 20, 1325–1343.

Coleman, D.S., Glazner, A.F., 1997. The Sierra Crest magmatic event: rapid formation of juvenile crust during the Late Cretaceous in California. International Geology Review 39, 768–787.

Coleman, D.S., Gray, W., Glazner, A.F., 2004. Rethinking the emplacement and evolution of zoned plutons: geochronologic evidence for incremental assembly of the Tuolumne Intrusive Suite, California. Geology 32, 433–436.

Connolly, J.A.D., Holness, M.B., Rubie, D.C., Rushmer, T., 1997. Reaction-induced microcracking: an experimental investigation of a mechanism for enhancing anatectic melt extraction. Geology 25, 591–594.

Cruden, A.R., 1988. Deformation around a rising diapir modeled by creeping flow past a sphere. Tectonics 7, 1091–1101.

Davidson, C., Hollister, L.S., Schmid, S.M., 1992. Role of melt in the formation of a deep-crustal compressive shear zone: the Maclaren Glacier metamorphic belt, South Central Alaska. Tectonics 11, 348–359.

Davis, M., 1996. Anisotropy of magnetic susceptibility and fabric analysis in granitoids: the Cascade Lake shear zone, Sierra Nevada, California. MS thesis, University of Minnesota, Minneapolis.

Dunlap, W.J., Hirth, G., Teyssier, C., 1997. Thermomechanical evolution of a ductile duplex. Tectonics 16, 983–1000.

Fleck, R.J., Kistler, R.W., Wooden, J.L., 1996. Geochronological complexities related to multiple emplacement history of the Tuolumne Intrusive Suite, Yosemite National Park, California: Geological Society of America Abstracts with Programs 28 (5), 65-66.

Fliervoet, T.F., White, S.H., Drury, M.R., 1997. Evidence for dominant grain-boundary sliding deformation in greenschist- and amphibolite-grade polymineralic ultramylonites from the Redbank Deformed Zone, Central Australia. Journal of Structural Geology 19, 1495–1520.

Freeman, B., 1987. The behavior of deformable ellipsoidal particles in three-dimensional slow flows: implications for geological strain analysis. Tectonophysics 132, 297–309.

Fry, N., 1979. Density distribution techniques and strained length methods for determination of finite strains. Journal of Structural Geology 1, 221–229.

Garlick, S.R., Gromet, L.P., 2004. Diffusion creep and partial melting in high temperature mylonitic gneisses, Hope Valley shear zone, New England Appalachians, USA. Journal of Metamorphic Geology 22, 45–62.

Gerbi, C., Johnson, S.E., Paterson, S.R., 2004. Implications of rapid, dike-fed pluton growth for host-rock strain rates and emplacement mechanisms. Journal of Structural Geology 26, 583–594.

Glazner, A., Bartley, J.M., Coleman, D.S., Gray, W., Taylor, R.Z., 2004. Are plutons assembled over millions of years by amalgamation from small magma chambers? GSA Today 14, 4–11.

Gower, R.J.W., Simpson, C., 1992. Phase boundary mobility in naturally deformed, high-grade quartzofeldspathic rocks: evidence for diffusional creep. Journal of Structural Geology 14, 301–313.

Greene, D.C., Schweickert, R.A., 1995. The Gem Lake shear zone: Cretaceous dextral transpression in the Northern Ritter Range pendant, eastern Sierra Nevada, California. Tectonics 14, 945–961.

Hibbard, M.J., 1987. Deformation of incompletely crystallized magma systems: granitic gneisses and their tectonic implications. Journal of Geology 95, 543–561.

Hirth, G., Tullis, J., 1992. Dislocation creep regimes in quartz aggregates. Journal of Structural Geology 14, 145–159.

Hirth, G., Teyssier, C., Dunlop, W.J., 2001. An evaluation of quartzite flow laws based on comparisons between experimentally and naturally deformed rocks. International Journal of Earth Sciences 90, 77–87.

Hollister, L.S., 1993. The role of melt in the uplift and exhumation of orogenic belts. Chemical Geology 108, 31–48.

Hollister, L.S., Crawford, M.L., 1986. Melt-enhanced deformation: a major tectonic process. Geology 14, 558–561.

John, B.E., Blundy, J.D., 1993. Emplacement-related deformation of granitoid magmas, southern Adamello massif, Italy. Geological Society of America Bulletin 105, 1517–1541.

Johnson, S.E., Fletcher, J.M., Fanning, C.M., Vernon, R.H., Paterson, S.R., Tate, M.C., 2003. Structure, emplacement and lateral expansion of the San José tonalite pluton, Peninsular Ranges batholith, Baja California, Mexico. Journal of Structural Geology 25, 1933–1957.

Karato, S., 1986. Does partial melting reduce the creep strength of the upper mantle? Nature 319, 309–310.

Kistler, R.W., Fleck, R.J., 1994. Field guide for a transect of the Central Sierra Nevada, California: geochronology and isotope geology. US Geological Survey, Open-File Report 94-267, 50 pp.

Kohlstedt, D.L., 1992. Structure, rheology and permeability of partially molten rocks at low melt fractions. In: Mantle Flow and Melt Generation at Mid-ocean Ridges. American Geophysical Union, Geophysical Monograph 71, 103–121.

Kruhl, J.H., 1996. Prism- and basal-plane parallel subgrain boundaries in quartz: a microstructural geothermometer. Journal of Metamorphic Geology 14, 581–589.

Marchildon, N., Brown, M., 2002. Grain-scale melt distribution in two contact aureole rocks: implications for controls on melt localization and deformation. Journal of Metamorphic Geology 20, 381–396.

McNulty, B.A., Tobisch, O.T., Cruden, A.R., Gilder, S., 2000. Multistage emplacement of the Mount Givens pluton, central Sierra Nevada Batholith, California. Geological Society of America Bulletin 112, 119–135.

McNulty, B.A., Tong, W., Tobisch, O.T., 1996. Assembly of a dike-fed magma chamber: the Jackass Lakes pluton, central Sierra Nevada, California. Geological Society of America Bulletin 108, 926–940.

Neves, S.P., Vauchez, A., Archanjo, C.J., 1996. Shear zone-controlled magma emplacement or magma-assisted nucleation of shear zones? Insights from northeast Brazil. Tectonophysics 262, 349–364.

Passchier, C.W., Trouw, R.A.J., 2005. Microtectonics. Springer-Verlag, Berlin, 366 pp.

Paterson, M.S., 2001. A granular flow theory for the deformation of partially molten rock. Tectonophysics 335, 51–61.

Paterson, S.R., Fowler Jr., T.K., 1993. Re-examining pluton emplacement processes. Journal of Structural Geology 15, 191–206.

Paterson, S.R., Okaya, D.A., 1999. Why don't we see more stoped blocks in plutons? Results from thermal-mechanical modeling. In: AGU 1999 fall meeting. EOS Transactions, American Geophysical Union 8, 983.

Paterson, S.R., Vernon, R.H., 1995. Bursting the bubble of ballooning plutons: a return to nested diapirs emplaced by multiple processes. Geological Society of America Bulletin 107, 1356–1380.

Paterson, S.R., Yu, H., 1994. Primary fabric ellipsoids in sandstones; implications for depositional processes and strain analysis. Journal of Structural Geology 16, 505–517.

Paterson, S.R., Miller, R.B., Anderson, J.L., Lund, S., Bendixen, J., Taylor, N., Fink, T., 1994. Emplacement and evolution of the Mount Stuart Batholith. In: Swanson, D., et al. (Eds.), Guides to Field Trips. Geological Society of America Annual Meeting, Seattle, Washington, pp. 2F-1–2F-48.

Paterson, S.R., Yu, H., Oertel, G., 1995. Primary and tectonic fabric intensities in mudrocks. Tectonophysics 247, 105–119.

Pignotta, G.S., Paterson, S.R., Pettersson, D., 2001. Voluminous stoping in the Mitchell Peak Granodiorite, Sierra Nevada, California. Cordilleran Section, 97th Annual Meeting, AAPG Pacific Section, Annual Meeting. Geological Society of America Abstracts with Programs 33, 64.

Poirier, J.P., 1985. Creep of Crystals. High-Temperature Deformation Processes in Metals, Ceramics and Minerals, Cambridge Earth Science Series. Cambridge University Press, Cambridge.

Ramsay, J.G., Huber, M.I., 1983. Strain Analysis. In: The Techniques of Modern Structural Geology, vol. 1. Academic Press, London, 307 pp.

Robin, P.Y., Cruden, A.R., 1994. Strain and vorticity patterns in ideally ductile transpression zones. Journal of Structural Geology 16, 447–466.

Rosenberg, C.L., 2001. Deformation of partially molten granite: a review and comparison of experimental and natural studies. International Journal of Earth Sciences 90, 60–76.

Rosenberg, C.L., Handy, M.R., 2000. Syntectonic melt pathways during simple shearing of a partially molten rock analogue (Norcampher-Benzamide). Journal of Geophysical Research 105, 3135–3149.

Rosenberg, C.L., Handy, M.R., 2005. Experimental deformation of partially melted granite revisited: implications for the continental crust. Journal of Metamorphic Geology 23, 19–28.

Rosenberg, C.L., Riller, U., 2000. Partial-melt topology in statically and dynamically recrystallized granite. Geology 28, 7–10.

Rushmer, T., 1995. An experimental deformation study of partially molten amphibolite: application to low-melt fraction segregation. Journal of Geophysical Research 100, 15681–15695.

Rushmer, T., 2001. Volume change during partial melting reactions: implications for melt extraction, melt geochemistry and crustal rheology. Tectonophysics 342, 389–405.

Rutter, E.H., 1997. The influence of deformation on the extraction of crustal melts: a consideration of the role of melt-assisted granular flow. In: Holness, M.B. (Ed.), Deformation-enhanced Fluid Transport in the Earth's Crust and Mantle. Chapman & Hall, London, pp. 82–110.

Rutter, E.H., Neumann, D.H.K., 1995. Experimental deformation of partially molten Westerly granite under fluid-absent conditions, with implications for the extraction of granitic magmas. Journal of Geophysical Research 100, 15697–15715.

Rutter, E.H., Casey, M., Burlini, L., 1994. Preferred crystallographic orientation development during the plastic and superplastic flow of calcite rocks. Journal of Structural Geology 16, 1431–1447.

Sawyer, E.W., 2001. Melt segregation in the continental crust: distribution and movement of melt in anatectic rocks. Journal of Metamorphic Geology 19, 291–309.

Schweickert, R.A., Lahren, M.M., 1993. Tectonics of the east-central Sierra Nevada- Saddlebag Lake and northern Ritter Range pendants. In: Lahren, M.M., Trexler, J.H., Spinoza, C. (Eds.), Crustal Evolution of the Great Basin and Sierra Nevada: Cordilleran-Rocky Mountain Section. Geological Society of America Guidebook, pp. 313–351.

Sharp, W.D., Tobisch, O.T., Renne, O.R., 2000. Development of Cretaceous transpressional cleavage synchronous with batholith emplacement, central Sierra Nevada, California. Geological Society of America Bulletin 112, 1059–1066.

Shimamoto, T., Ikeda, Y., 1976. A simple algebraic method for strain estimation from deformed ellipsoidal objects; 1, Basic theory. Tectonophysics 36, 315–337.

Spear, F.S., 1993. Metamorphic phase equilibria and pressure-temperature-time paths. Mineralogical Society of America Monograph Series 1, 799.

Stipp, M., Stünitz, H., Heilbronner, R., Schmid, S.M., 2002. The eastern Tonale fault zone: a 'natural laboratory' for crystal plastic deformation of quartz over a temperature range from 250 to 700 °C. Journal of Structural Geology 24, 1861–1884.

Stocker, R.L., Ashby, M.F., 1973. On the rheology of the upper mantle. Reviews of Geophysics and Space Physics 11, 391–426.

Stöckhert, B., Brix, M.R., Kleinschrodt, R., Hurford, A.J., Wirth, R., 1999. Thermochronometry and microstructures of quartz – a comparison with experimental flow laws and predictions on the temperature of the brittle-ductile transition. Journal of Structural Geology 21, 351–369.

Tikoff, B., de Saint Blanquat, M., 1997. Transpressional shearing and strike-slip partitioning in the Late Cretaceous Sierra Nevada magmatic arc, California. Tectonics 16, 442–459.

Tikoff, B., Teyssier, C., 1992. Crustal-scale, en-echelon "P-shear" tensional bridges: an example from the Sierra Nevada batholith California. Journal of Structural Geology 19, 29–39.

Tikoff, B., Davis, M.R., Teyssier, C., de St Blanquat, M., Habert, G., Morgan, S., 2005. Fabric studies within the Cascade Lake shear zone, Sierra Nevada, California. Tectonophysics 400, 209–226.

Tobisch, O.T., Fiske, R.S., Saleeby, J.B., Holt, E., Sorensen, S.S., 2000. Steep tilting of metavolcanic rocks by multiple mechanisms, central Sierra Nevada, California. Geological Society of America Bulletin 112, 1043–1058.

Tobisch, O.T., Renne, P.R., Saleeby, J.B., 1993. Deformation resulting from regional extension during pluton ascent and emplacement, central Sierra Nevada, California. Journal of Structural Geology 15, 609–628.

Tobisch, O.T., Saleeby, J.B., Fiske, R.S., 1986. Structural history of continental volcanic arc rocks, eastern Sierra Nevada, California: a case for extensional tectonics. Tectonics 5, 65–94.

Tobisch, O.T., Saleeby, J.B., Renne, P.R., McNulty, B., Tong, W., 1995. Variations in deformation fields during development of a large-volume magmatic arc, central Sierra Nevada, California. Geological Society of America Bulletin 107, 148–166.

Tommasi, A., Vouchez, A., Fernandes, L.A.D., Porcher, C.C., 1994. Magma-assisted strain localization in an orogen-parallel transcurrent shear zone of southern Brazil. Tectonics 13, 421–437.

Twiss, R.J., Moores, E.M., 1992. Structural Geology. W.H. Freeman and Company, New York, 532 pp.

van der Molen, I., Paterson, M.S., 1979. Experimental deformation of partially-melted granite. Contributions to Mineralogy and Petrology 70, 229–318.

Vernon, R.H., 1991. Questions about myrmekite in deformed rocks. Journal of Structural Geology 13, 979–985.

Wahrhaftig, C., 2000. Geologic map of the Tower Peak quadrangle, central Sierra Nevada, California. In: Ciener, J.S (Ed.), compiled by Huber, N.K. 1998. Geologic Investigation Series I-2697, US Geological Survey.

Webber, C.E., Candela, P.A., Piccoli, P.M., Simon, A.C., 2001. Generation of granitic dikes: can texture, mineralogy, and geochemistry be used as guides to determine the mechanism of diking? Geological Society of America Abstracts with Programs 33, A-138.

Yoshinobu, A., Marko, W., Dumond, G., Wolak, J., Barnes, C., Nordgulen, O. 2003. Stoping happens! Geological Society of America Abstracts with Programs 35, 93.

Yoshinobu, A.S., Girty, G.H., 1999. Measuring host rock volume changes during magma emplacement. Journal of Structural Geology 21, 111–116.

Žák, J., Paterson, S.R., 2005. Characteristics of internal contacts in the Tuolumne Batholith, central Sierra Nevada, California (USA): implications for episodic emplacement and physical processes in a continental arc magma chamber. Geological Society of America Bulletin 117, 1242–1255.

Zulauf, G., 2001. Structural style, deformation mechanisms and paleodifferential stress along an exposed crustal section; constraints on the rheology of quartzofeldspathic rocks at supra- and infrastructural levels (Bohemian Massif). Tectonophysics 332, 211–237.